Journal of Materials Chemistry A

ROYAL SOCIETY OF CHEMISTRY

PAPER

View Article Online
View Journal | View Issue

Cite this: *J. Mater. Chem. A*, 2026, **14**, 17957

Intrinsic microstructures of C-A-S-H and N(-C)-A-S-H gels at low Ca/Si and Si/Al ratios

Yulin Deng[abc] and Zuhua Zhang *[abcd]

Received 4th December 2025
Accepted 20th March 2026

DOI: 10.1039/d5ta09930g

rsc.li/materials-a

Understanding the microstructures of low calcium aluminosilicate hydrate (C-A-S-H) and calcium containing sodium aluminosilicate hydrate (N(-C)-A-S-H) is essential for the performance prediction and therefore manufacturing of geopolymers, or more broadly, chemically activated aluminosilicate cements. This study aims to reveal their atomic ordering and molecular structure using synthetic C-A-S-H/N(-C)-A-S-H gels at low Ca/Si (0–1.0) and Si/Al (1–2) ratios. High energy XRD with pair distribution function (PDF) analysis, TEM, and $^{29}Si/^{27}Al$ NMR analysis show that Ca concentration is a more governing factor than Al in governing the overall Si/Al evolution of gels. Distinct Q^1 and Q^2 structural units are formed under the conditions of Si/Al > 1.75 and Ca/Si $\geq$ ~0.2–0.5. Ca and Al exhibit synergistic/antagonistic effects on Si tetrahedral units: Al increases Q^4 (enhancing polymerization), while Ca promotes Q^2 (improving ordering) but reduces Q^3 (decreasing connectivity). An estimation calculation formula linking the proportion of Q^4 sites to Si/Al and measured Ca/Si ratios of products is established to simplify the determination of C-A-S-H and N(-C)-A-S-H gel proportions in alkali-activated systems (including low-Ca hybrid alkaline cement). The new insights into C-A-S-H and N-A-S-(H) gel microstructures enable future work to better understand the relationship between phase composition and geopolymer performance. The findings elucidate the interactions and mechanisms of elemental composition governing gel evolution, with implications for geopolymer manufacturing and application.

1. Introduction

Geopolymers, or more broadly, chemically activated cement, are widely regarded as greener alternatives to ordinary Portland cement (OPC) due to their lower CO_2 emissions during processing and the valorization of industrial wastes.[1–3] The reaction mechanisms of geopolymers generally involve three steps, including dissolution of aluminosilicates, gel nucleation, and polycondensation.[4] The products are either calcium containing sodium aluminosilicate hydrate (N(-C)-A-S-H) for low Ca precursors, calcium (alumino)silicate gels (C-A-S-H) for high Ca precursors, or a mixture of them when blended precursors are used.[5] Designing and manufacturing a durable geopolymer remains challenging due to compositional variability in precursors and curing procedures.[6–8]

Geopolymers are known to be susceptible to a variety of harmful degradation phenomena, including shrinkage, microcracking and large creep.[9–11] Given that the gels in geopolymers are mostly amorphous, it is likely that their stability is partly responsible for the various degradation mechanisms. From a thermodynamic point of view, (nano)crystal gels are more stable than amorphous ones, so the formed C-A-S-H and N(-C)-A-S-H gels are inherently less thermodynamically stable than the products of OPC. Ye and Radlińska[12] found that the incorporation of alkali cations might reduce the regularity of C-A-S-H layer stacking through ionic size differences, making C-A-S-H easier to collapse and redistribute during drying. This leads to a special concern on the shrinkage and creep issues of geopolymers. In addition, the increase of aluminum content is accompanied by the increase of alkali ions, as the deficit due to the replacement of Si^{4+} with Al^{3+} ions in a tetrahedral structure at the bridging site must be balanced through the adsorption/binding of alkali cations in the interlayer.[13] Zhang *et al.*[14] recently proposed the concept of phase engineering, and as a demonstration, they added calcined layered double hydroxide (CLDH) powder as a seed into the slag-based geopolymer, transforming the microstructure from a typical amorphous gel into a more ordered C-A-S-H gel and more hydrotalcite nanocrystals. The mechanical properties and water retention of geopolymers doped with nanocrystalline seeds were improved,

[a]*Key Laboratory for Green & Advanced Civil Engineering Materials and Application Technology of Hunan Province, College of Civil Engineering, Hunan University, Changsha 410082, P. R. China. E-mail: zhangzuhua@tongji.edu.cn*

[b]*International Science Innovation Collaboration Base for Green & Advanced Civil Engineering Materials of Hunan Province, Hunan University, Changsha 410082, P. R. China*

[c]*Key Laboratory of Building Safety and Energy Efficiency of the Ministry of Education, Hunan University, Changsha 410082, China*

[d]*Key Laboratory of Advanced Civil Engineering Materials of Ministry of Education, School of Materials Science and Engineering, Tongji University, Shanghai, 201804, P. R. China*

and the autogenous shrinkage and drying shrinkage were significantly reduced.[15]

The variation of the atomic composition and molecular structure of C-(A)-S-H and N(-C)-A-S-H is the most fundamental reason that affects the performance of geopolymers, apart from the coagulation mode of gel particles. Increasing the Ca/Si ratio leads to more stacking layers in the main sheets and thicker nanoscale structural units, which significantly reduces the specific surface area.[16] When the Ca/Si ratio increases from 0.6 to 1.6, the specific surface area decreases from approximately 430 $m^2 g^{-1}$ to 180 $m^2 g^{-1}$.[17] In addition, increasing Ca/Si ratio results in a thicker and more fibrillar gel morphology.[18] When Al is incorporated, the increased negative charge density and the formation of interlayer aluminate hydrates lead to larger basal spacing and interlayer distances in the gel.[19,20] As the Al/Si ratio increases from 0 to 0.05 and then to 0.2, the specific surface area first increases from ~50 $m^2 g^{-1}$ to ~110 $m^2 g^{-1}$, but subsequently drops to ~15 $m^2 g^{-1}$.[21] For decalcified samples, the specific surface area keeps increasing from about 120–220 $m^2 g^{-1}$ to 350–650 $m^2 g^{-1}$ when Al content increases.

Li *et al.*[22] found that the addition of metakaolin provided additional soluble Si and Al to the reaction system and reduced the concentrations of Na^+ and OH^- in the pore solution. This led to the early formation of N(-C)-A-S-H gel, while delaying the formation of C-A-S-H and the development of a pore structure, and slowed down the driving force of autogenous shrinkage. Wang *et al.*[23] found that the decrease of the Ca/Si ratio of C-A-S-H from 1.2 to 0.8 slightly increased the creep coefficient, which can lead to a lower creep deformation. When the Al/Si ratio decreased from 0.3 to 0, the creep coefficient increased or first increased and then decreased. The negative effect of Al addition on creep may come from the higher crosslinking degree of the aluminosilicate structure. However, this mechanism is not clear so far. Myers *et al.*[24] proposed a C-A-S-H model to describe the compositional continuum of geopolymer gels. However, the atomic-scale structure, particularly the roles of Ca and Al in the Al-rich and Ca-deficient environment, remains incompletely validated. Advanced characterization techniques, such as high-energy XRD and PDF analysis, have revealed the local ordering in C–S–H for OPC and C-A-S-H/N-A-S-H gels for alkali-activated GGBS/metakaolin.[25,26] White *et al.*[27] used PDF to identify distinct Si–O–Si/Si–O–Al bond-length distributions in alkali-activated GGBS pastes. They found that both calcium and aluminum contents in the raw materials would reduce the degree of (alumino)silicate polyhedra connectivity. These findings emphasize the necessity and demand for fundamental research on gels at the atomic scale.

Moreover, previous research has found that gel phases with different Ca/Si and Si/Al ratios can exist simultaneously.[28,29] Walkley *et al.*[30] found that the rise of Al content promoted the formation of calcium carboaluminate AFm phases and generated additional N-A-S-H gel. However, at Ca/Si ratios less than 0.8, the evolution of gels, the structure of the Si–O–Si/Si–O–Al unit, and Al substitution in the gel framework remain unclear, due to changes in elemental composition and the complex effect of Al and Ca. In addition, the diversity of precursor preparation and selection methods can enhance the incorporation of aluminum into the gel structure.[31] However, the coexistence of gels in aluminum-rich environments remains unclear.

This study aims to reveal the intrinsic microstructures of C-A-S-H and N(-C)-A-S-H gels. Here, N(-C)-A-S-H refers to a N-A-S-H gel without or with a low concentration of Ca present in various forms. To achieve this goal, gels with controlled Ca/Si and Si/Al ratios are synthesized *via* a chemical precipitation method. The effects of the Ca/Si ratio, Si/Al ratio and reaction time on the molecular structures and morphological evolution of C-A-S-H and N(-C)-A-S-H gels are investigated using high energy XRD plus PDF, TEM and $^{29}Si/^{27}Al$ NMR analysis. Al coordination and its impact on gel crosslinking are discussed together with the mean chain length *via* Q^n speciation analysis. The findings of this paper are of great significance for understanding the formation of various geopolymer gels with different calcium, sodium, silicon and aluminum contents and provide critical insights into geopolymer formulation design.

2. Experimental program

2.1. Raw materials

In this study, N(-C)-A-S-H and C-A-S-H gels were synthesized by a sol–gel method. Previous studies have confirmed that the synthetic gels could present similar structural properties to those obtained in geopolymer and related alkali-activated cements.[29,32,33] The chemical reagents used in the experiment included sodium metasilicate nonahydrate ($Na_2SiO_3 \cdot 9H_2O$), calcium nitrate tetrahydrate ($Ca(NO_3)_2 \cdot 4H_2O$), aluminum nitrate nonahydrate ($Al(NO_3)_3 \cdot 9H_2O$) and sodium hydroxide (NaOH). The above reagents were analytically pure, and the experimental water was laboratory ultra-pure water. Two ratios of Si/Al were set as 1.0 and 2.0 in this experiment to simulate high and low Al products. The Ca/Si ratios were set as 0, 0.1, 0.2, 0.3, 0.4, 0.5, 0.6, 0.8, and 1.0, respectively, to represent no calcium to low calcium products.

2.2. Gel synthesis

150 mL of Na_2SiO_3 solution and 150 mL of a mixed solution of $Ca(NO_3)_2$ and $Al(NO_3)_3$ were prepared according to the molar composition in Table 1 at 20 °C. The mixed solution of $Ca(NO_3)_2$ and $Al(NO_3)_3$ was gradually added into Na_2SiO_3 solution using

Table 1 Molar composition of synthetic gels

Si/Al	Ca/Si	Si/Al	Ca/Si
2	0	1	0
	0.1		—
	0.2		0.2
	0.3		—
	0.4		0.4
	0.5		0.5
	0.6		0.6
	0.7		—
	0.8		0.8
	1.0		1.0

a peristaltic pump at a rate of 2 mL min^{-1}, accompanied by continuous stirring. At a relatively low pH value (<12.5), the content of SiO_2 and the degree of polymerization in the formed gel can be higher than those in typical Portland cement gels, and silica gel may be formed in the absence of calcium.[33] Thus, to maintain the pH of the reaction solution above 13, NaOH solution was added to Na_2SiO_3 solution. The mixed solution was left to react for 1 day, 28 days and 90 days before solid–liquid separation. The separated solid was then washed multiple times using about 1 L of deionized water each time to remove the unreacted substances. It is worth noting that residual unreacted species may remain in the filtrate. Previous studies have shown that in synthetic gels with Si/Al ratios ranging from 1 to 3, over 95% of the aluminum is incorporated into the reaction products.[34] This indicates a strong affinity of aluminum for incorporation into the solid N-A-S-H gel structure. After being washed and filtered using filter paper with a pore size of 74 μm, the solid samples were vacuum-dried and stored in a vacuum container under ambient temperature conditions. It should be noted that the actual elemental composition of the gel may not be the same as the designed composition. The subsequent molecular structure analysis will be based on the measured Ca/Si ratios.

2.3. Gel characterization

2.3.1 Normal X-ray diffraction (XRD) analysis. Normal XRD analysis was conducted using an X'Pert powder X-ray diffractometer, using Cu-Kα radiation with $\lambda = 0.154$ nm. The scanning range was 5° to 60° 2θ with a step size of 0.02° and a scanning speed of 2° min^{-1}.

2.3.2 High energy XRD test plus pair distribution function (PDF) analysis. Synchrotron radiation was applied for X-ray scattering on the BL13w and SSRF-BL14B1 beam lines at room temperature, at the Shanghai Synchrotron Radiation Facility (SSRF). Each powder sample was placed into a cylindrical borosilicate glass tube with a diameter of 1 mm. Then, the tube was sealed, mounted, and rotated several times to calibrate the position. The test time for each sample varied between 15 and 30 min, depending on the test energy. Two energy levels were used: 69.5 keV with radiation $\lambda = 0.178$ Å and 18 keV with radiation $\lambda = 0.6887$ Å. The data were calibrated using a CeO_2-filled tube and an empty tube. The program Fit2D was used for the data conversion from 2D to 1D.[35] In PDF analysis, $G(r)$ is obtained by taking a sine Fourier transform of the measured total scattering function, $S(Q)$, where Q is the momentum transfer. The PDF data were obtained using PDFgetX3,[36] with a Q_{max} of 10–20 $Å^{-1}$.

2.3.3 Fourier transform infrared (FTIR) spectra analysis. For the FTIR test, 0.001 g of the powder sample was mixed with 0.1 g of dried potassium bromide (KBr), followed by gentle grinding and pressing into a transparent pellet. FTIR spectra were acquired using a Thermo Scientific IS10 spectrometer (Thermo Fisher Scientific, USA). The spectra were recorded over the range of 4000 to 400 cm^{-1} at a resolution of 2 cm^{-1}, with a total of 64 scans co-added.

2.3.4 Scanning electron microscope (SEM) analysis. The powder sample was dispersed onto a pre-cut carbon tape strip, gently purged with nitrogen gas to eliminate any loosely adhered particles, and subsequently sputter-coated with gold to ensure adequate electrical conductivity. Imaging was conducted using a TESCAN-MIRA3 LMH field emission scanning electron microscope operated at an accelerating voltage of 20 kV and equipped with a One Max 20 detector for energy dispersive spectrometer (EDS) analysis.

2.3.5 Transmission electron microscope (TEM) analysis. TEM analysis was conducted by using a Themis Z TEM instrument with an energy dispersive spectrometer (EDS) detector. It was performed at an energy of 80 kV and a pixel resolution of <0.136 nm was carried out. The morphology and the elemental composition of a specific region of the powder sample could be acquired.

2.3.6 ^{27}Al and ^{29}Si magic-angle spinning nuclear magnetic spectroscopy (MAS NMR). MAS NMR experiments were performed on a Bruker AVANCE III 600 spectrometer at a resonance frequency of 119.2 MHz. The spectra with high-power proton decoupling were recorded on a 4 mm probe with a spinning rate of 10 kHz, a π/4 pulse length of 2.6 μs, and a recycle delay of 40 s. Deconvolution was performed using a Gauss–Lorentzian curve for each component. The peaks of spectra were identified, and the background was removed. The deconvolution was between −70 ppm and −120 ppm for ^{27}Si spectra, and −10 ppm and 90 ppm for ^{27}Al spectra, to investigate the interaction/coordination between various Si and Al species.

3. Results and discussion

3.1. Phase assemblies of synthetic gels

The XRD patterns of the synthetic gels are given in Fig. 1. The impact of Ca content on gel structure ordering (crystallinity) is evident. At 1 day, for the gels with a designed Si/Al atomic ratio of 2, when Ca/Si ≤ 0.2, a wide diffraction hump appears near 29° 2θ, without other characteristic peaks. This indicates that the synthetic products are amorphous phases. The location and shape of the peak are consistent with those of the diffraction peak of hydration products in alkali-activated metakaolin or low-calcium fly ash geopolymers,[37–39] indicating that the synthetic gels are similar to N-A-S-H gels. When the Ca/Si ratio increases to 0.3, a diffraction peak with low intensity appears at 29°, which gradually becomes sharper and stronger with the increase of the Ca/Si ratio, accompanied by a decrease in the diffraction hump of N-A-S-H gel. When the Ca/Si ratio reaches 0.4, weak but clear characteristic peaks appear at 29°, 31°, 50° and 55°. These characteristic peaks correspond to C(-A)-S-H gel phases (PDF# 00-029-0331 (ref. 40) and PDF# 00-030-0227), and the intensities of diffraction peaks are gradually enhanced with the increase of Ca/Si. The characteristic peaks at ∼27°, 32° and 39.4° 2θ can be attributed to katoite. When katoite contains Si, peaks should occur within the 2θ value range of ∼39.6° to ∼40°; thus, it is inferred that the katoite here is silica-free (C_3AH_6, ICSD 94630).[41] In addition, no new diffraction peaks appear in the synthetic gels with Ca/Si > 1.0, according to our last research.[29] For the gels with a designed Si/Al ratio of 1, the center of the broad diffraction hump still appears at 29° 2θ, which means that the systems obtain a gel similar to that

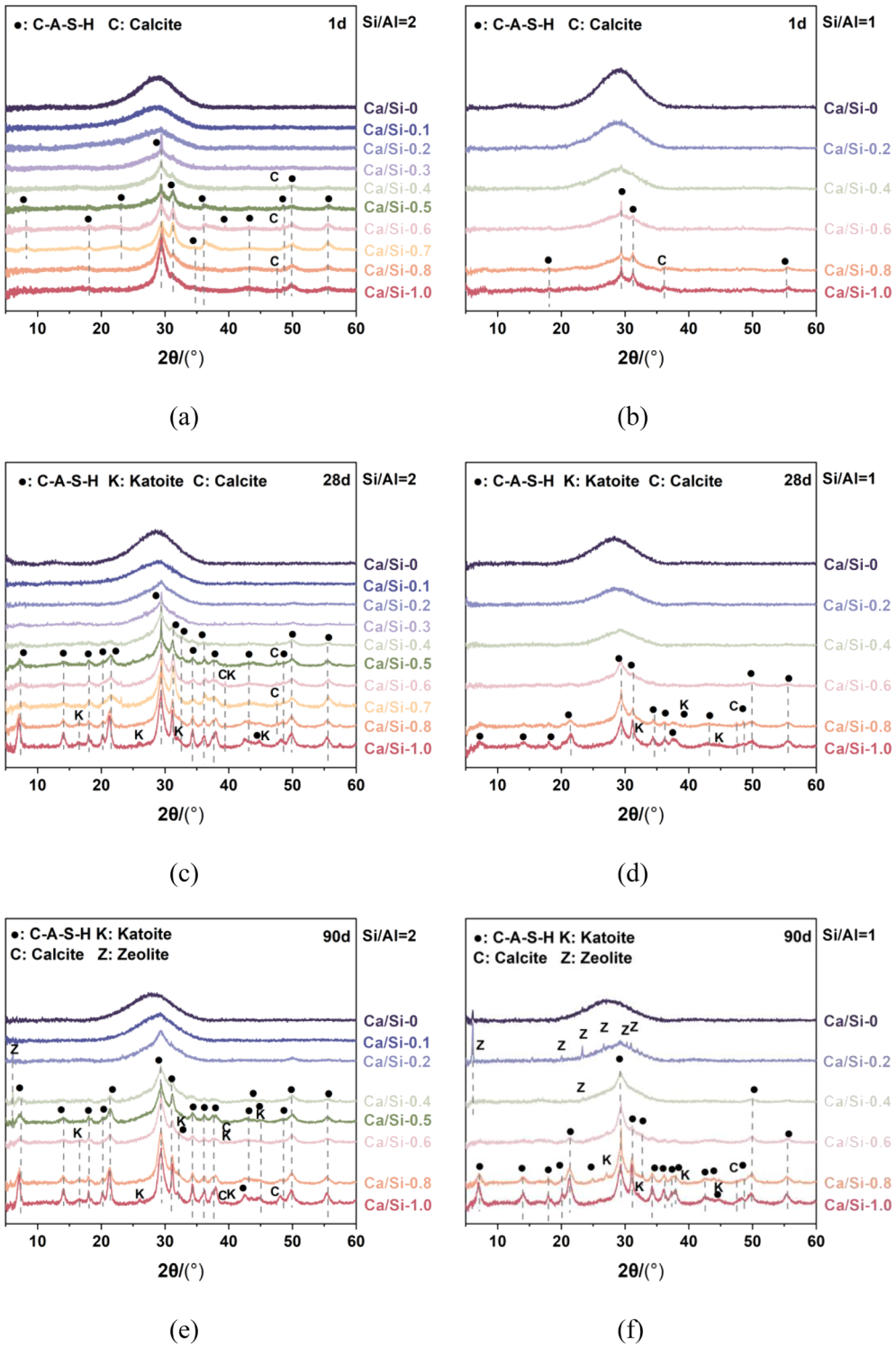

Fig. 1 XRD patterns of the synthetic gels after reaction for (a and b) 1 day, (c and d) 28 days, and (e and f) 90 days at Si/Al ratios of 1 and 2.

obtained at Si/Al = 2. The C-A-S-H diffraction peak appears after 90 days, which is much later than its appearance at 1 day at Si/Al = 2. In general, the XRD peaks of the synthetic gels change regularly as the Ca/Si ratio increases from 0 to 1.0.

The results of XRD analysis show that N-A-S-H gel is gradually transformed into hydrated calcium aluminosilicate gel with the increase of Ca/Si, and the initial broad diffraction hump is transformed into a sharp diffraction peak. C-(A)-S-H is composed of nanocrystals and an amorphous matrix. These nanocrystals exhibit a distinct layered structure. Based on the results of SEM images (see Appendix A), it can be observed that as the Ca/Si ratio increases, the Si/Al ratio decreases, and the reaction time increases, some thin sheet-like and needle-like products with better crystallinity appear in the gel. This

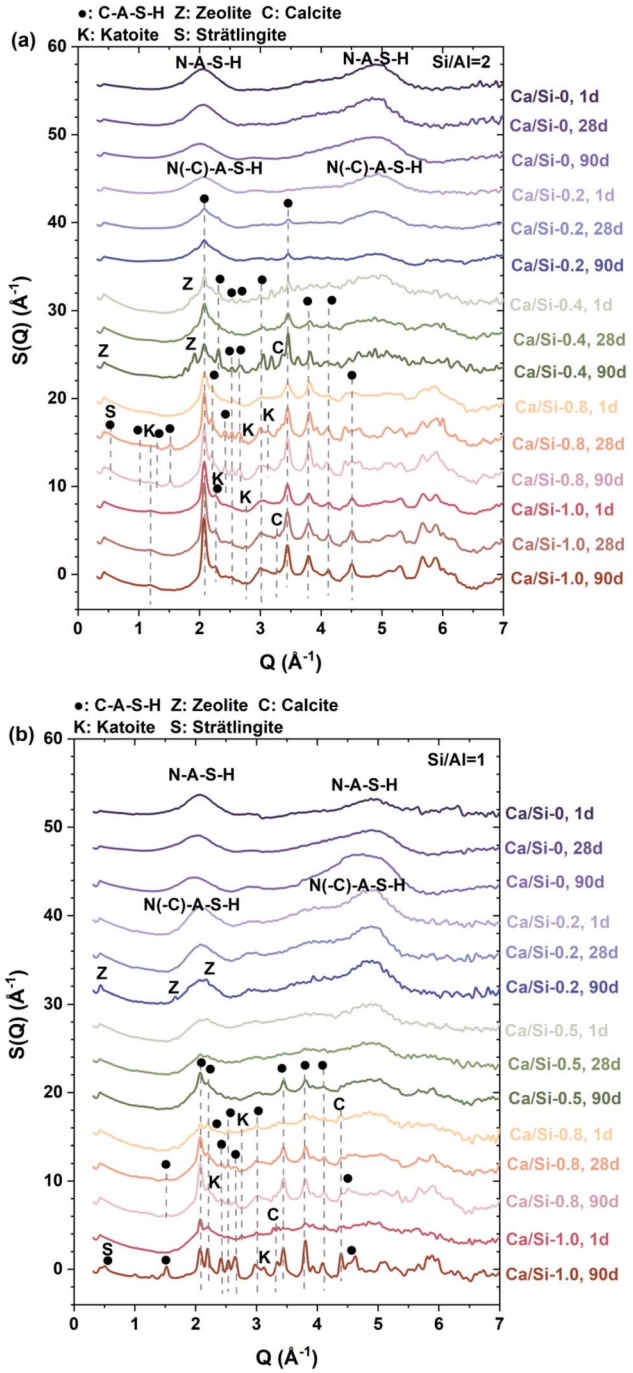

Fig. 2 X-ray total scattering functions of gels: (a) Si/Al = 2 and (b) Si/Al = 1.

indicates that the increase of Ca/Si leads to the gradual ordering of synthetic gel. Si *et al.*[42] investigated the effect of calcium content on alkali-activated metakaolin. They found that the incorporation of calcium ions can re-order the atomic structure of the alkali-activated materials and enhance the crystallization. Gao *et al.*[43] found that with the increase of slag content, the alkali-activated paste showed a lower content of newly formed Q^4 groups in the main products. The alkali-activated slag-fly ash system can change from N-A-S-H gel to C-A-S-H gel, with the increase of Ca concentration in precursors. A large number of calcium ions promoted the formation of the C-A-S-H gel phase.

A new finding is the time dependency of crystallization of N-A-S-H gel. As the reaction time increases to 28 and 90 days, a zeolite phase ($Na_{88}Al_{88}Si_{104}O_{384}(H_2O)_{220}$, PDF#01-070-2168) is detectable for gels with Ca/Si < 0.4. The crystallinity of C-A-S-H also improves. This means that even under sol–gel reaction conditions (much more homogeneous than real geopolymerization systems), both N-A-S-H and C-A-S-H undergo slow structural reorganization, becoming more ordered. It implies that for geopolymers and related materials, this phase reorganization must be considered under low Ca/Si conditions. In addition, a reduction of the Si/Al ratio leads to broadened diffraction peaks of gels, demonstrating that Al incorporation induces structural disorder in the gel network and disrupts the long-range structural ordering.

The incorporation of alkali metals leads to significant modifications in the solid-phase composition. E. L'Hôpital *et al.*[41] found that C–S–H, strätlingite, katoite and aluminium hydroxide could be observed without alkali metals at Si/Al ratios of 3 to 5 and Ca/Si ratios of 0.8 to 1. Meanwhile, in the presence of potassium ions, the reaction products are dominated by substantial C-A-S-H gel and katoite, with very small amounts of strätlingite and portlandite. Walkley *et al.*[30] reported the formation of N-A-S-H, C-A-S-H, AFm type phases, and portlandite at Si/Al ratios of ~6.6 to ~20 and Ca/Si ratios of ~0.7 to ~1.1 in the presence of Na. In this study, at low Si/Al ratios of 1 to 2, zeolite can be identified at Ca/Si ≤ 0.4, while katoite can be observed at Ca/Si ratios of 0.5 to 1. This finding is essential for the understanding of the macroscale performance of such low Ca/Si and Si/Al cementitious materials.

3.2. Atomic ordering of C-A-S-H and N(-C)-A-S-H gels

Fig. 2 shows the X-ray total scattering patterns of the synthetic gels. In comparison with the XRD results in Fig. 1, there are more detailed diffraction peaks found in low Ca/Si ratios, such as 0.2 and 0.4. This means that the high energy diffraction is more effective for identifying the local structures of C-A-S-H and N(-C)-A-H gels.

To further investigate the local atomic ordering within the microstructures of gels, PDF analysis is applied, and the quantitative analysis results are shown in Fig. 3. The date below ~1 Å (below the first Si/Al–O correlation) are the result of experimental noise, imperfect background correction and termination error.[44] The PDF peaks located at below ~5 Å are related to the atom–atom correlations of the amorphous phase of the tested materials. The peak between 4 and 5 Å is difficult to allocate due to the overlapping atom–atomic correlation in this region, while the peak at ~4.3 Å may be attributed to the second Si/Al–O atom–atomic correlation.[27] The features in the range of $5 \leq r \leq 8$ Å provide the middle range ordering of gels, and those at $10 \leq r \leq 40$ Å can give the long-range ordering. The nanocrystalline ordering of gels is observed at large r values, *i.e.*, $6 \leq r \leq 40$ Å.[26,45]

The first peak at ~1.65 Å is composed of contributions of Si–O and Al–O bonds. The Al here might be tetra-coordinated,

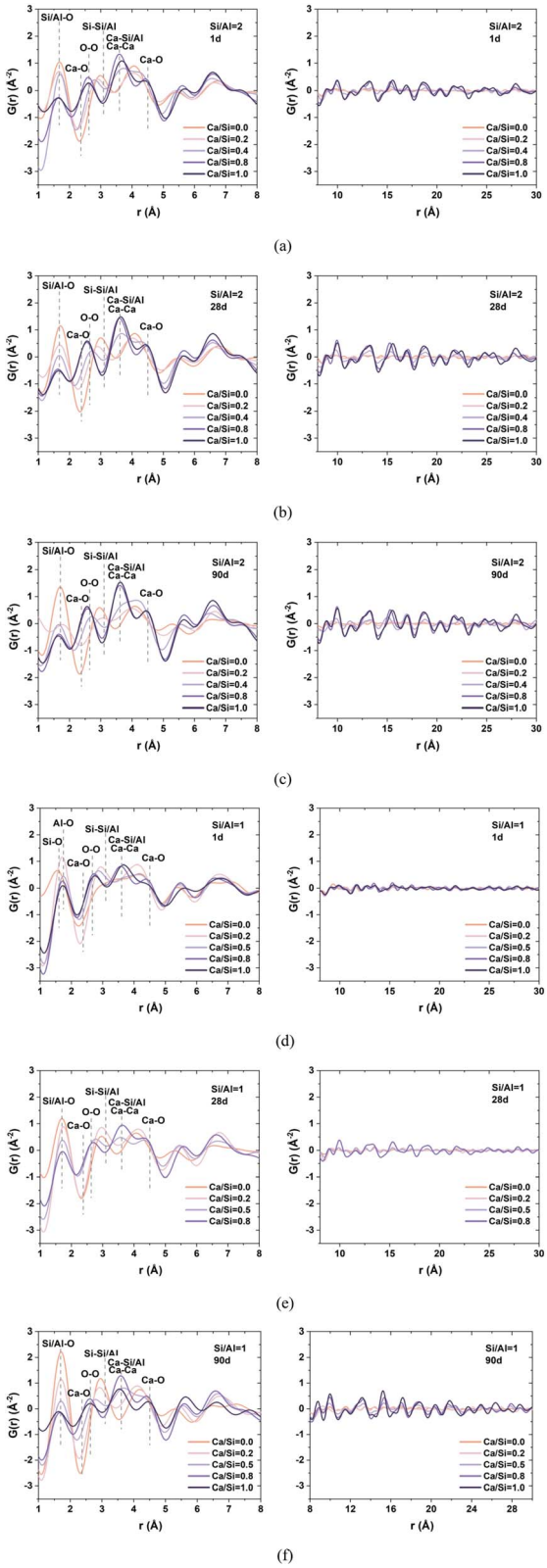

Fig. 3 X-ray total scattering functions of gels with Si/Al = 2 and Si/Al = 1 after reaction for (a and b) 1 day, (c and d) 28 days, and (e and f) 90 days.

because the Al^{V}–O bond distances can be longer.[25] At Ca/Si = 0, the first Si/Al–O peak is sharper when the Si/Al ratio is lower, especially at longer reaction times (see Fig. 3(e) and (f)). This indicates that the disorder of this coordination environment decreases with increasing Al and the atomic arrangement of N-A-S-H gel tends towards the ideal lattice position with time.

The addition of Ca makes this atom–atom correlation distance smaller. Soyer-Uzun *et al.*[46] found that as the Ca concentration or the age increased, the Si–Si/Al peak moved towards a higher *r* value and became narrower, which indicates a higher extent of crystallization.[46] However, this can also be attributed to the increase in aluminum content in the amorphous phase. The atom–atom correlation at ~1.72 Å can be attributed to Al–O, which was slightly larger than the Si–O distance in tetrahedrally coordinated silica (~1.60 Å).[25,26,45] Thus, the shift of Si/Al–O towards a lower *r* with increasing Ca concentration is mainly affected by the reduced amount of Al in gel, which counteracts the effect of gel polymerization on the first Si/Al–O peak. In addition, in comparison to the samples with Si/Al = 1, this Si/Al–O peak for those with a Si/Al ratio of 2 shows a greater extent of decline with increasing Ca concentration. Thus, the addition of Ca seems to have a great effect on the Si/Al–O bond in the sample with less Al content.

The second peak is attributed to Ca–O, O–O and Si–Si/Al correlation. The Ca–O correlation is at ~2.35 Å, and the O–O correlation is at ~2.65 Å. The Si–Si/Al correlation at ~3.15 Å is associated with the bonds between tetrahedral Si units and tetrahedral or higher coordination Al.[25] White *et al.*[47] compared the differences between high alkali-activated metakaolin and low alkali-activated slag. The Si/Al–O and Si–Si/Al peaks were sharper when Ca concentration was absent. Similarly, the effect of Ca–O correlation gradually appears and becomes more evident with the increase of the Ca/Si ratio, causing a significant shift in the second peak, especially when Si/Al = 2. The second Ca–O correlation becomes evident at ~4.5 Å.[48] In Fig. 4(b), the Si–Si/Al peak moves to higher *r* values with the increase of Ca and the decrease of Al content. The intensity of the Si–Si/Al correlation in C-(N)-A-S-H gel represents the connectivity of the silica and alumina units.[27] Thus, the Si/Al ratio seems to have a greater impact on the connectivity of aluminosilicate gel compared to Ca or Na when Ca/Si ≤ 0.4.

White *et al.*[26] found that C-A-S-H and C-S-H gels were both nanocrystalline, with only minor differences above 5 Å. However, Fig. 3 shows that gels with Ca/Si ≤ 0.5 exhibit almost no long-range ordering beyond 8 Å, confirming their amorphous nature, especially when the reaction time is short. This confirms that for gels with low Ca content and high Al content, the features at large *r* values show significant differences.

The framework connectivity (degree of polymerization) of gel, *e.g.* (Si–Si/Al)/(Si/Al–O) ratio, is calculated for analyzing the aluminosilicate gels. Accurately determining this ratio necessitates the clear identification of both the Si–Si/Al and Si/Al–O peaks; therefore, a minimum test energy of ~58 keV ($\lambda = 0.2114$ Å)[27] is required for this calculation. The connectivity values are 0.426 for Ca/Si = 0.2, Si/Al = 1 at 1 day, 0.382 for Ca/Si = 0.4, Si/Al = 2 at 1 day, and 0.355 for Ca/Si = 0.4, and Si/Al = 2 after 90 days, respectively. With the increase of calcium content, the

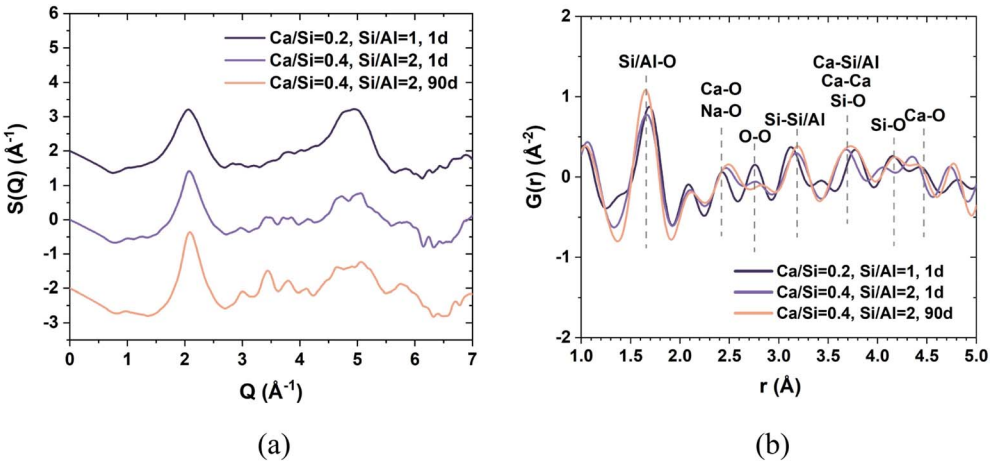

Fig. 4 (a) X-ray scattering patterns and (b) PDFs of gels tested at 69.5 keV.

decrease of aluminum content and the increase of age, the gel connectivity declines. These connectivity values are close to that in alkali-activated metakaolin (~0.4) and alkali-activated slag pastes (0.2–0.6) but higher than that in C-S-H gel.[25–27,47,49]

3.3. Micromorphology of phase assemblies

Fig. 5 and 6 respectively show the TEM images of the synthetic gels with different Ca/Si ratios from 1 day to 90 days. These results confirm that the Ca/Si ratio plays a critical role in the morphology and phase composition of the synthetic gels. At 1 day, when the Si/Al ratio is 2, increasing the Ca/Si ratio induces notable structural changes. The N-A-S-H gel displays a cotton-like structure, as shown by TEM-EDS. When Ca/Si = 0.2, irregular granular structures emerge. Although this new phase contains a certain amount of calcium (Ca/Si ratio of 0.26), the actual measured Si/Al ratio of 1.5 and the presence of sodium make it more likely to be N(-C)-A-S-H gel rather than C-A-S-H gel. It is noted that the calcium-free cotton-like N-A-S-H gel coexists with this granular phase. At Ca/Si = 0.4, calcium-free N-A-S-H gel disappears. N(-C)-A-S-H and C-A-S-H gels seem to coexist without phase separation, accompanied by the actual Ca/Si ratio increasing to 0.38, the Na/Si ratio decreasing to approximately 0.1 and the Si/Al ratio remaining unchanged. A previous study has also found that phase separation still exists at 1 day when the Ca/Si ratio is 0.4;[29] however, compared with the findings in this study, the phase separation principle should be Si/Al ratio dependent. This highlights the importance of the role of Al in determining the phase morphology and assembly. When Ca/Si increases to 0.8, the detected phase Si/Al ratio significantly increases to ~2.5, featuring irregular granular and lamellar features characteristic of C-A-S-H gel. It is proven that N-A-S-H and N(-C)-A-S-H dominate in low-calcium systems with Ca/Si < 0.4.

Similar trends are observed in samples with designed Si/Al = 1. The Ca-free N-A-S-H gels exhibit a uniform cotton-like structure. When the Ca/Si ratio increases to 0.2, a uniform particle phase of N(-C)-A-S-H can be obtained. Compared to that with the same initial Ca concentrate but Si/Al = 2, the detected Si/Al ratio is reduced to approximately 1.25, and the Ca/Si ratio decreases to 0.18. The results indicate a competitive incorporation mechanism of Al and Ca into the gels. For samples of Ca/Si ≥ 0.4, the gels transition to C-A-S-H gradually with a low Na

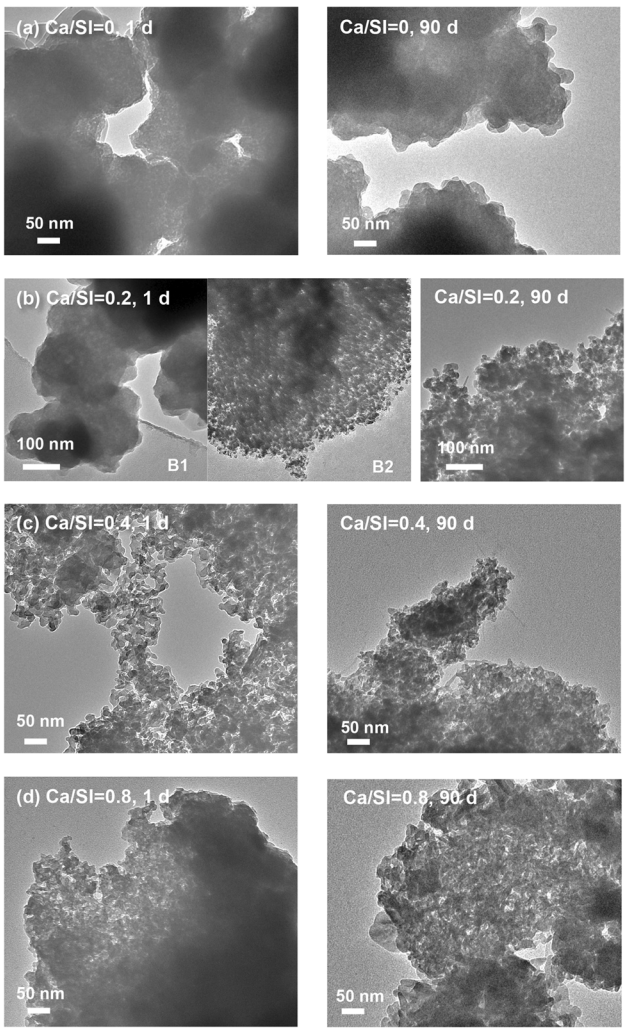

Fig. 5 TEM images of synthetic gels with designed Ca/Si ratios of (a) 0, (b) 0.2, (c) 0.4, and (d) 0.8 at 1 day and 90 days when Si/Al = 2.

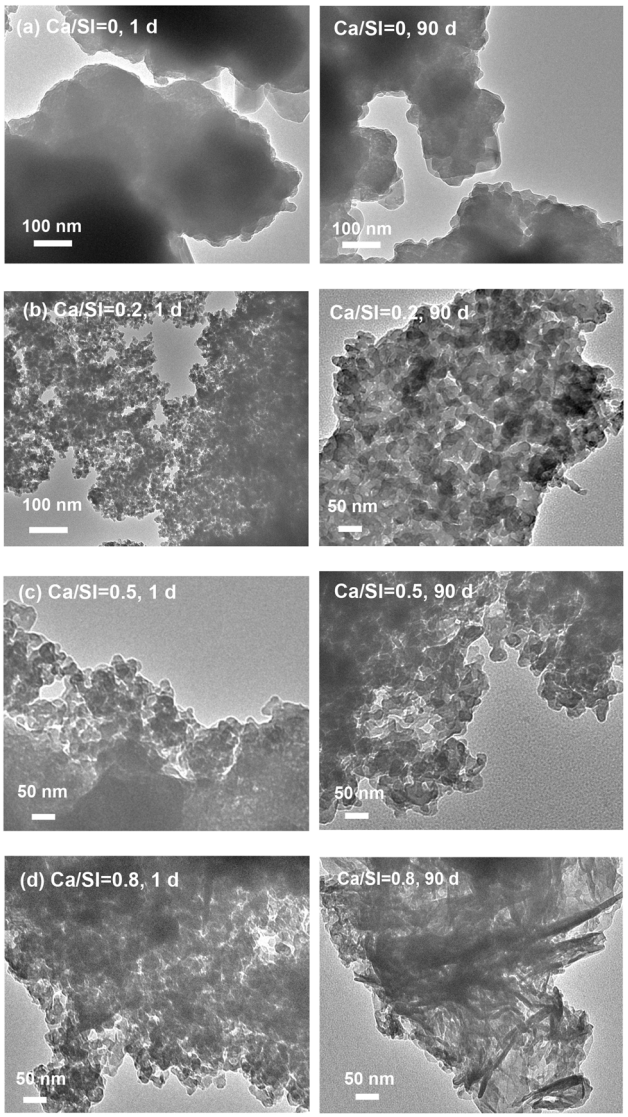

Fig. 6 TEM images of synthetic gels with designed Ca/Si ratios of (a) 0, (b) 0.2, (c) 0.4, and (d) 0.8 at 1 day and 90 days when Si/Al = 1.

concentration. When the reaction time is 1 day, Na still exists in the gel with a Na/Si ratio of ~0.15. After 90 days, the Na concentration becomes extremely low. This demonstrates the progressive expulsion of Na from the system over time with increasing Ca concentration. The low detected Si/Al ratio of 1.7 suggests the existence of N(-C)-A-S-H or calcium aluminate hydrate (AFm) phases. Thus, N(-C)-A-S-H and C-A-S-H coexist with morphological differences only under specific Si/Al and Ca/Si ratios at early ages, and this behavior heavily depends on reaction time and Ca concentration.

The Si/Al ratio also affects gel stability and phase evolution. When Ca/Si = 0, with increased aluminum incorporation, a reduction in the Na/Si ratio is observed, suggesting potential Na^+ substitution by Al^{3+} in the structure. At a low Si/Al ratio, gels show greater homogeneity, with N(-C)-A-S-H forming at Ca/Si = 0.2.

After 90 days of reaction, phase separation completely disappears in all the calcium-containing samples. The gel structure of N-A-S-H remains cotton-like and becomes denser. The low-calcium system shows smaller granular structures over time, accompanied by the disappearance of cotton-like N-A-S-H structures. When the Ca/Si ratio increases to 0.8, the gel exhibits a mixed structure of foil-shaped and granular forms. Prolonged reaction time prevents N-A-S-H gel from existing as a stable, separate phase in calcium-containing systems. The residual Na and low Si/Al ratios after 90 days still suggest the possible existence of the N(-C)-A-S-H gel framework, which may become morphologically mixed with C-A-S-H gel (Table 2).

3.4. Functional group analysis by FTIR

Fig. 7 and 8 present the FTIR spectra of samples with different Ca/Si ratios cured for 1 day and 90 days, respectively. The characteristic band assignments of the main functional groups can be identified across the spectra.

For all samples, a broad band located at approximately 2900–3700 cm^{-1} is attributed to the stretching vibration of O–H (ν O–H) groups associated with vibration water and structural hydroxyls in products.[50] The spectra also feature a band at around 3620 cm^{-1}, which corresponds to the O–H stretching of silanol groups. Meanwhile, the band around ~1640 cm^{-1} corresponds to the deformation vibration (δ O–H) of free water and chemically bound water.[51,52] With decreasing Ca/Si ratio, the intensity of the O–H stretching band becomes slightly enhanced, indicating an increase in bound water or hydroxyl-containing gel phases.

The band at approximately 1400–1500 cm^{-1} is assigned to the stretching vibration of C–O bonds in CO_3^{2-} groups,[53] suggesting the presence of carbonate species formed by carbonation during curing or sample preparation. The intensity of this band becomes slightly more pronounced at higher Ca/Si ratios, implying that Ca-rich systems seem to be more susceptible to carbonation.

In the range of 840–1200 cm^{-1}, a prominent band corresponding to the asymmetric stretching vibration of Si–O–T (T = Si or Al) bonds[54,55] can be observed, which is associated with the aluminosilicate network in C-N-A-S-H/N-A-S-H gels. As the Ca/Si ratio increases, this band gradually shifts toward lower wavenumbers, indicating a reduction in the polymerization degree of the aluminosilicate framework and the progressive incorporation of Ca into the gel structure, leading to the formation of C-N-A-S-H gel. In contrast, samples with lower Ca/Si ratios exhibit relatively higher wavenumbers, reflecting a more polymerized N-A-S-H-dominated network.

The bands at ~720 cm^{-1} correspond to the deformation vibrations of Si–O–Al linkages within the aluminosilicate framework.[51,56] The bands located at approximately 660 cm^{-1} are attributed to the deformation vibrations of Si–O–Si bonds.[57] The bands in the region of 550–620 cm^{-1} correspond to the deformation vibrations of Si–O–T linkages within the aluminosilicate framework.[52,54] In addition, the bands located at approximately 550 cm^{-1} are attributed to the deformation vibrations of Si–O bonds in SiO_4 tetrahedra.[58] These bands are present in all samples, confirming the formation of tetrahedrally coordinated silicate structures and the incorporation of Al into products.

Table 2 Atomic percentage ratios of synthetic gels with various designed Si/Al and Ca/Si ratios after reaction for 1 day and 90 days as measured by TEM-EDS mapping

Designed Si/Al	Designed Ca/Si	Age (d)	Detected Si/Al ratio	Detected Na/Si ratio	Detected Ca/Si ratio
2	0	1	1.27	0.49	—
		90	1.26	0.70	—
	0.2	1-B1	1.38	0.65	—
		1-B2	1.47	0.26	0.13
		90	1.48	0.22	0.20
	0.4	1	1.71	0.07	0.38
		90	2.35	0.01	0.37
	0.8	1	2.56	—	0.62
		90	2.94	—	0.68
1	0	1	1.35	0.47	—
		90	0.96	0.46	—
	0.2	1	1.35	0.40	0.18
		90	1.19	0.02	0.32
	0.5	1	1.27	0.11	0.33
		90	1.69	0.01	0.51
	0.8	1	1.43	0.03	0.47
		90	1.98	0.04	0.77

Comparing the two systems, both Si/Al = 2 and Si/Al = 1 samples exhibit similar functional group characteristics; however, the band positions in the Si–O–T region show slightly lower wavenumbers for the Si/Al = 2 system, indicating a relatively lower degree of silicate polymerization and Al involvement. Overall, the FTIR results demonstrate that the gel structure evolves from a highly polymerized aluminosilicate network toward a Ca-modified aluminosilicate gel with increasing Ca/Si ratio.

3.5. Molecular structure of products

3.5.1 Al status in N(-C)-A-S-H and C-A-S-H. The ^{27}Al MAS NMR spectra for the synthetic gels after the reaction for 1, 28, and 90 days are shown in Fig. 9. Two types of aluminates, four-coordinate Al(IV) at 50–80 ppm and six-coordinate Al(VI) at 0–20 ppm, are found in the synthetic gels. The spectrum primarily features tetrahedrally coordinated Al sites. When the Ca/Si ratio of gel is low, bridged silicate species tend to be replaced by Al(IV) species; when the Ca/Si ratio is high, more Al(VI) and Al(V) species might appear.[59] However, Al(V) cannot be detected in this research, which might be due to the low incorporation amount of Ca.

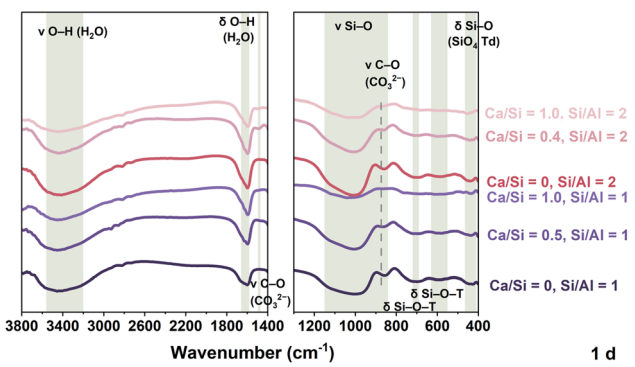

Fig. 7 FTIR spectra for samples reacted for 1 day.

3.5.1.1 Al(IV) species. The tetrahedrally coordinated Al sites are the predominant form in gels. In this study, the resonance at about 61.5 ppm is assigned to Al(IV) species in N-A-S-H gel, which could also be found in zeolite.[60] Walkley *et al.*[61] found that the Al(IV) resonance at $\delta_{cg} = 62.4$ ppm could be attributed to Si(IV)–O–Al(IV) linkages in N-A-S-H gel, which is balanced by Na^+ or extra-framework Al(IV) species.

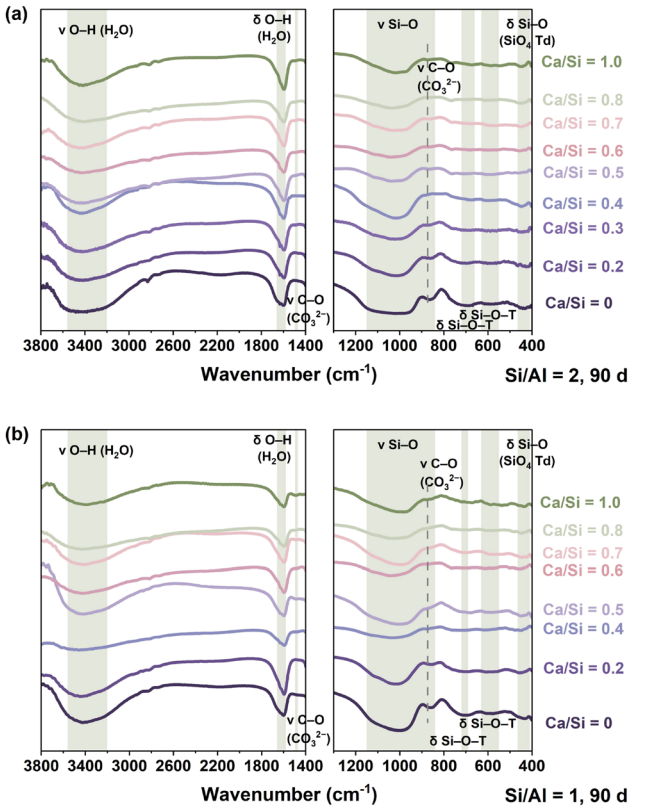

Fig. 8 FTIR spectra for samples reacted for 90 days: (a) Si/Al = 2 and (b) Si/Al = 1.

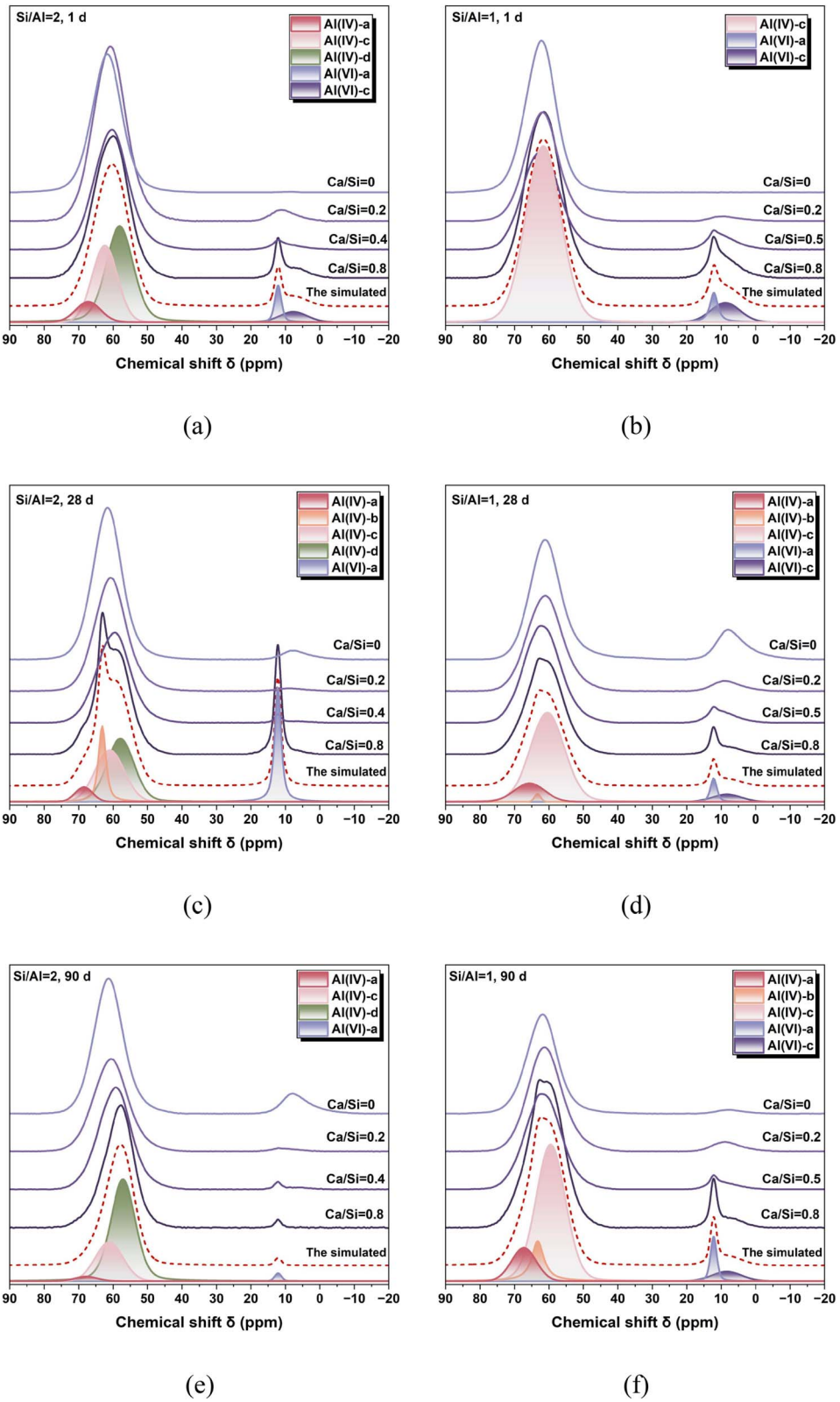

Fig. 9 ^{27}Al MAS NMR spectra and deconvolution of the synthetic gels with designed Si/Al = 2 and Si/Al = 1 after reaction for (a and b) 1 day, (c and d) 28 days, and (e and f) 90 days.

In C-A-S-H gel, the presence of multiple Al(IV) species has been reported. Small cations charge-compensating aluminates induce lower Al resonance frequencies, whereas larger cationic species result in higher resonance frequencies.[62] This arises because large cations (*e.g.*, Ca^{2+}) disrupt the coordination sphere symmetry through long-range electrostatic fields.

Previous studies have identified that the Al resonances observed at 60–75 ppm may originate from Q^2(1Al) bridging site units. In addition, the resonance at ~58 ppm can be attributed to Al in Q^3(Al) units (cross-linking sites).[19] Specifically:

(1) The resonance at ~75 ppm represents bridging Al(IV) species charge-balanced by nearby Na^+ ions,[63] Ca^{2+} ions[59] or interlayer/surface Al(VI) and Al(V) species.[19]

(2) The resonance at 66–68 ppm is attributed to bridging Al(IV) charge-balanced by $\frac{1}{2}Ca^{2+}$ together with H_3O^+ groups[63] or by small ions (*e.g.*, H^+).[59]

(3) The resonance at ~61 ppm is attributed to bridging Al(IV) balanced by interlayer Ca^{2+} ions either alone or in combination with Na^+ ions,[63] while the resonance at 62 ppm may represent Q^3 coordinated Al.[64]

The Al(IV)-a site appearing at a relatively high chemical shift of ~68 ppm is assigned to Q^2 Al at chain-bridging sites balanced by $\frac{1}{2}Ca^{2+}$ together with H_3O^+ ions or by H^+ ions. This is consistent with the decreasing trend of Al(IV)-a with the increase of calcium content. The Al(IV)-c site at ~61 ppm is attributed to bridging Q^2 Al charge-balanced *via* interlayer Ca^{2+} ions or combinations of interlayer Ca^{2+} and Na^+ ions. The Al(IV)-c site at ~61 ppm is also assigned to Al(IV) species in N-A-S-H gel. The Al(IV)-d site at ~58 ppm is attributed to the cross-linked Q^3 Al site. The Al resonance associated with pairing Al(IV) is not taken into account because pairing Al is energetically unfavored and a consensus has not been reached.[65]

3.5.1.2 Al(VI) species. A low Si/Al ratio may lead to the formation of secondary phases, such as zeolites, katoite ($Ca_3Al_2(OH)_{12}$), calcium aluminate hydrate (AFm) phases (*e.g.*, strätlingite, a siliceous AFm-type phase, $2CaO{\cdot}Al_2O_3{\cdot}SiO_2{\cdot}8H_2O$), and alumina gel ($Al(OH)_3$). The Al(VI)-a and Al(VI)-b sites occur with the increase of reaction time and Ca/Si ratio. This indicates that these Al(VI) sites are affected by Ca concentration. The Al(VI)-a site at ~12 ppm can be attributed to aluminates of the AFt phase,[63] AFm phase,[24] or katoite.[41] The Al(VI)-b site at ~10.5 ppm can be attributed to the AFm phase (*e.g.*, hemicarbonate, $Ca_4Al_2(OH)_{13}{\cdot}0.5CO_3{\cdot}xH_2O$; monocarbonate, $Ca_4Al_2(OH)_{12}{\cdot}CO_3{\cdot}xH_2O$; hydroxy-AFm phase, C_4AH_{13}; C_2AH_6),[19,30] calcium aluminate hydrates ($CaAl_2(OH)_8{\cdot}6H_2O$, $Ca_2Al_2(OH)_{10}{\cdot}3H_2O$, and $Ca_4Al_2(OH)_{14}{\cdot}6H_2O$), katoite, or siliceous hydrogarnets.[41,63] In addition, Al(IV)-b′ at ~63 ppm is assigned to the Al within strätlingite[19] when Si/Al = 2. The comparable proportions of Al(VI)-a and Al(IV)-b′ species prove that they both belong to the AFm phase. To deconvolute the overlapping signals of Al(IV)-c and Al(IV)-b′ in the ~61–63 ppm region, the Al(VI)-a peak serves as a key reference. Both Al(VI)-a and Al(IV)-b′ are associated with the AFm phase, which is preferentially formed in samples with a higher Si/Al ratio. Therefore, the presence of Al(VI)-a provides indirect evidence for the existence of Al(IV)-b′. This assignment is further supported by the distinctly sharper shape of the Al(IV)-b′ peak.

However, when the Si/Al ratio is 1, after reaction for 90 days, the proportion of the peak Al(IV)-b at ~63 ppm reaches the highest and is disproportionate to that of Al(VI)-a at 12 ppm. This suggests that the peak at ~63 ppm likely corresponds to bridging Q^2 Al(IV) species when the Si/Al ratio = 1 and the reaction time is 90 days. This finding is also consistent with the subsequent deconvolution results of the ^{29}Si NMR spectra, which reveal the highest proportion of Q^2(Al) species under conditions of Ca/Si = 0.5 after 90 days of reaction.

The intensity of the Al(VI)-c site at ~8 ppm can be seen in almost all N-A-S-H spectra and reduces with the increase of Ca content. This site may be linked to the Al(VI) within paragonite.[66] The contents or crystallization degrees of paragonite might be so low that they are not detectable in the normal XRD pattern.

3.5.2 Si connection in N(-C)-A-S-H and C-A-S-H. Fig. 10 shows ^{29}Si MAS NMR spectra of the synthetic N-A-S-H gels without Ca after reaction for 1, 28, and 90 days. Quantification of each deconvoluted spectral resonance was performed using Gaussian peak fitting, with partial resulting component peaks and simulated spectrum presented in Fig. 10 alongside the data in Tables 5 and 6.

The resonance at −76 ppm can be attributed to Q^0 monomers,[63] suggesting the existence of a small number of remnants

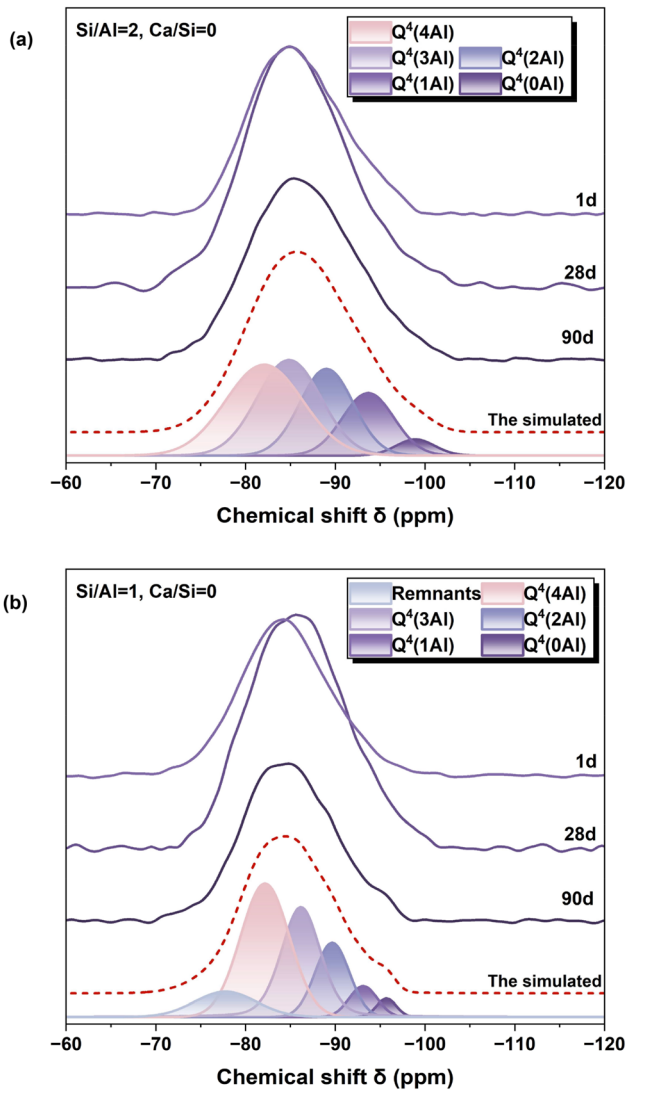

Fig. 10 ^{29}Si MAS NMR spectra and deconvolution of the synthetic N-A-S-H gels with (a) designed Si/Al = 2 and (b) designed Si/Al = 1 after reaction for 1, 28 and 90 days. The simulated curves (dashed line) represent the two 90 day samples.

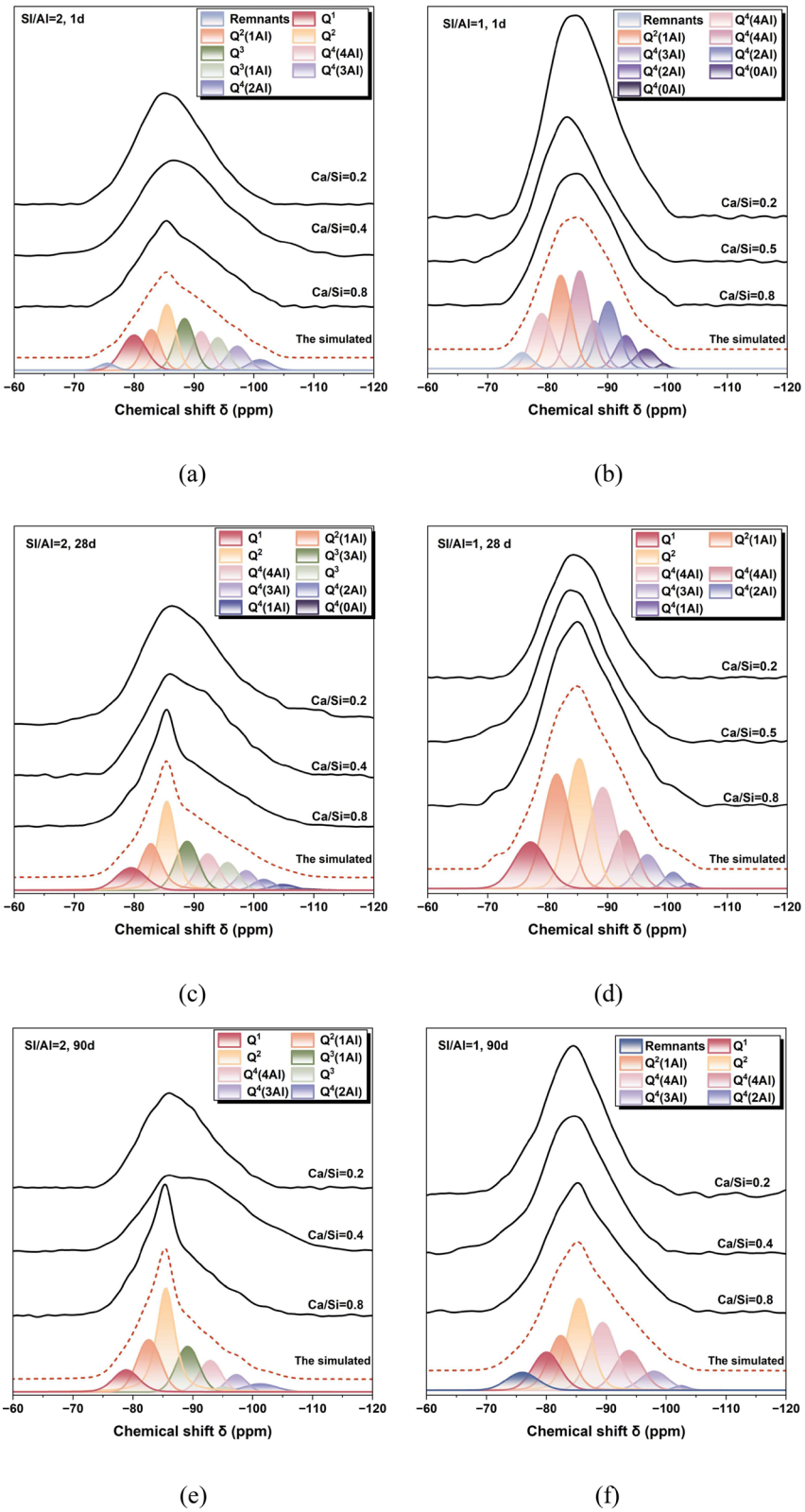

Fig. 11 ^{29}Si MAS NMR spectra and deconvolution of synthetic gels with designed Si/Al = 2 and Si/Al = 1 after reaction for (a and b) 1 day, (c and d) 28 days, and (e and f) 90 days. The simulated curves (dashed line) represent the samples of Ca/Si = 0.8.

of the initial sodium silicate.[67] Five Si environments of N-A-S-H gel are characterized by the varied peaks at approximately −81 ppm, −86 ppm, −89 ppm, −93 ppm, and −96.5 ppm, corresponding to Q^4(4Al), Q^4(3Al), Q^4(2Al), Q^4(1Al), and Q^4(0Al), respectively. The spectra of gels at different reaction times are similar because the N-A-S-H gels all contain the distribution of

Q^4 (mAl) sites. These Q^4 sites also exist in the ^{29}Si MAS NMR spectra of alkali-activated fly ash (with a low CaO content) or metakaolin pastes,[68,69] while the proportion of individual Q^4 resonances is more due to the complex chemical environment and the presence of unreacted precursors.

Fig. 11 shows the ^{29}Si MAS NMR spectra and deconvolution results of synthetic gels with Ca incorporated. There are multiple distinct possibilities in terms of bonding environments of non-bridging oxygens, which may influence the ^{29}Si chemical shift of a Q^1 site, rather than this simply being determined by whether the single bridging oxygen atom is linked to Si or Al. Bernal *et al.*[70] assigned the resonances at −77 ppm and −80 ppm to Q^1 sites in alkali-activated slag pastes, considering that the Q^1 sites can be bonded to Si or Al and can also have different ratios of Ca^{2+}, Na^+ and H^+ in charge-balancing sites. Zhu *et al.*[59] assigned the peak at −77 ppm to Q^2p(Al(VI)), a paired silicate tetrahedra neighboring a substituted octahedral aluminate.[21] However, the possible corresponding Al-resonance is not found (at ∼5 ppm) or its developmental trend in this research does not conform to the previous study (at ∼9 ppm), as discussed in Section 3.5.1. In crosslinked C-A-S-H gel, the substituted Al is considered to exist only in the form of Al(IV). Thus, in this study, the center of the resonances between −78 and −80 ppm is assigned to the Q^1 site. The resonances at about −82 ppm (corresponding to Q^2(1Al) sites) and −85 ppm (Q^2 sites) are consistent with the formation of a tobermorite-like structured C-A-S-H gel.

It must be noted that deconvolutions of the spectra have been previously reported in many studies.[19,66,67] A commonly accepted guiding principle is that the intensities of adjacent Q^4(mAl) peaks should change smoothly, rather than exhibiting a much higher or lower intensity for a specific Q^4(mAl) site than that of adjacent (m + 1 or m − 1) sites. This principle was introduced on the thermodynamic basis of the statistical distribution of Si and Al sites in the Q^4 (glass or gel) network.[71] Although the site population is not directly obtained from such a distribution, this principle is applied here to ensure that the deconvolution results are meaningful.[70]

The center positions and widths of peaks are generally kept constant during the deconvoluting process. However, by comparing the spectra and deconvolution results of gel without Ca and that with Ca/Si ≥ 0.58, a change in the position of Q^4(mAl) peaks can be observed.[30,66] For instance, the peak center value of Q^4(4Al) is −84.5 ppm in N-A-S-H gel with Si/Al = 1.5 or 2.5, while it is −88 ppm in C–N-A-S-H gel. Thus, the center position of the Q^4(mAl) peak in ^{29}Si MAS NMR spectra is not a fixed value due to the significant changes in Si Q^4(mAl) environments caused by the variations in calcium and aluminum concentrations.

Previous studies have shown that the chemical shifts of Q^4(mAl) in N-A-S-H gel and Q^2(mAl) together with Q^3(mAl) in C-A-S-H gel in ^{29}Si MAS NMR spectra overlap.[70] For instance, the peaks at −89 ppm can be assigned to Q^3(Al) and Q^4(4Al) of C-A-S-H gel and that at −93 ppm can be assigned to Q^3 and Q^4(3Al) species.[30] For the gel with a relatively high Ca/Si ratio (approximately higher than 0.6) and a high Si/Al ratio, peaks can be assigned to Q^2, Q^3, and Q^4 straightforwardly through the difference in the chemical shift of ^{29}Si NMR spectra deconvolution results. It is challenging to distinguish Q^2, Q^3, and Q^4 for the synthetic gels for which Ca/Si and Si/Al ratios are both low, especially when the peak position cannot be fixed. Therefore, it is assumed that the change in each peak position of Q^4(mAl) is gradual when the Ca/Si ratio increases. The deconvolution results of gels with Ca/Si = 0.8 and without Ca in this study are consistent with existing studies. Thus, the maximum and minimum values of the chemical shift of each Q^4(mAl) with the general variation trend can be determined. In addition, in this study, when determining the peak distribution of Q^2, Q^3 or Q^4 of C-A-S-H gel, the Si/Al ratio of gel obtained from TEM-EDS is taken as a reference. The Si/Al ratios obtained from TEM-EDS are compared with those from the deconvolution results. Only the results that have a good match between peak distribution and TEM-EDS results are adopted. It should be noted that when Ca exists in gel, though a certain peak might be assigned to Q^4, a small number of Q^2 or Q^3 may actually exist in the molecule due to the overlap of chemical shifts.

The ^{29}Si NMR spectra provide the relative intensities of different tetrahedral Si sites (Q^1, Q^2, and Q^3), enabling the calculation of the mean chain length (MCL) of non-crosslinked and crosslinked gel molecules. The calculation equations of the MCL of the C-A-S-H phase and the Si/Al ratios of N(-C)-A-S-H and C-A-S-H gels are as follows:[24]

$$\mathrm{MCL_{NC}} = \frac{2\left(\mathrm{Q^1} + 3/2\mathrm{Q^2(Al)} + \mathrm{Q^2}\right)}{\mathrm{Q^1}} \quad (1)$$

$$\mathrm{MCL_{C}} = \frac{4\left(\mathrm{Q^1} + \mathrm{Q^2(Al)} + \mathrm{Q^2} + \mathrm{Q^3} + 2\mathrm{Q^3(1Al)}\right)}{\mathrm{Q^1}} \quad (2)$$

$$\mathrm{Si/Al_{NASH}} = \frac{\sum_{m=0}^{4} \mathrm{Q^4}(m\mathrm{Al})}{\sum_{m=0}^{4} \frac{m}{4}\mathrm{Q^4}(m\mathrm{Al})} \quad (3)$$

$$\mathrm{Si/Al_{NC\text{-}CASH}} = \frac{2\left(\mathrm{Q^1} + \mathrm{Q^2(Al)} + \mathrm{Q^2}\right)}{\mathrm{Q^2(Al)}} \quad (4)$$

$$\mathrm{Si/Al_{C\text{-}CASH}} = \frac{\mathrm{Q^1} + \mathrm{Q^2(Al)} + \mathrm{Q^2} + \mathrm{Q^3} + \mathrm{Q^3(1Al)}}{\mathrm{Q^3(1Al)}} \quad (5)$$

where NC and C denote non-crosslinked and crosslinked C-A-S-H gel structures.

The $\mathrm{Si/Al_{entire}}$ ratio of entire synthetic substances (including Si remnants) is calculated from the results of ^{29}Si NMR. For comparison purposes, with the $\mathrm{Si/Al_{entire}}$ ratio, the $\mathrm{Si/Al_{Al\ NMR}}$ values are calculated using the fractions of Al(IV) obtained from ^{27}Al NMR spectra and the $\mathrm{Si/Al_{TEM}}$ ratios obtained from the TEM test. The equations are as follows:

When Q^1, Q^2(mAl), and Q^3(mAl) units are absent:

$$\mathrm{Si/Al_{entire}} = 1 \Big/ \frac{I_{\mathrm{Q^4}}}{\mathrm{Si/Al_{NASH}}} \quad (6\text{-}1)$$

When Q^3(mAl) units are absent:

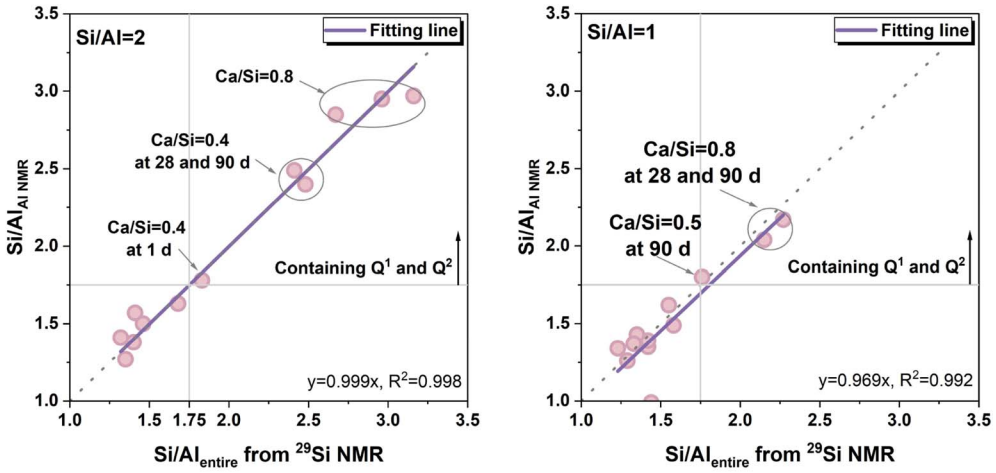

Fig. 12 Relationship between the Si/Al_{entire} ratio from ^{29}Si NMR and the $Si/Al_{Al\ NMR}$ ratio from ^{27}Al NMR and TEM-EDS results for the synthetic gels with (a) Si/Al = 2 and (b) Si/Al = 1 after reaction for 1, 28 and 90 days. The dashed line represents a 1 : 1 correlation.

$$Si/Al_{entire} = 1 \Big/ \left(\frac{I_{Q^{12}}}{\frac{Si}{Al}_{NC\text{-}CASH}} + \frac{I_{Q^4}}{\frac{Si}{Al}_{NASH}} \right) \quad (6\text{-}2)$$

When all the Q^1, $Q^2(mAl)$, $Q^3(mAl)$, and $Q^4(mAl)$ units are present:

$$Si/Al_{entire} = 1 \Big/ \left(\frac{I_{Q^{123}}}{\frac{Si}{Al}_{C\text{-}CASH}} + \frac{I_{Q^4}}{\frac{Si}{Al}_{NASH}} \right) \quad (6\text{-}3)$$

$$Si/Al_{Al\ NMR} = \frac{Si/Al_{TEM}}{I_{Al(IV)\text{-}gel}} \quad (7)$$

where $I_{Q^{12}}$, $I_{Q^{123}}$ and I_{Q^4} represent the fractions of $Q^1 + Q^2(mAl)$, $Q^1 + Q^2(mAl) + Q^3(mAl)$ and $Q^4(mAl)$ Si units from ^{29}Si NMR spectra deconvolution; $I_{Al(IV)\text{-}gel}$ is the fraction of Al(IV) in gels of the total Al(IV) + Al(VI) species from ^{27}Al NMR spectra; Si/Al_{TEM} is the Si/Al ratio obtained from the TEM test. The calculated MCL of C-A-S-H and the Si/Al ratios of N-A-S-H and C-A-S-H gels are given in Table 7, providing substantial information to understand the molecular structure of the synthetic gel from an average perspective view.

Fig. 12 shows good agreement between the Si/Al_{entire} ratio from ^{29}Si NMR spectra and the $Si/Al_{Al\ NMR}$ ratio calculated from ^{27}Al NMR spectra and TEM analyses. In Fig. 12(a), the Si/Al_{entire} ratio and $Si/Al_{Al\ NMR}$ ratio show a good linear correlation. It should be noted that this study adopts the widely adopted classification, where Q^1, Q^2, and Q^3 Si units belong to C-A-S-H gel and Q^4 Si units belong to N-A-S-H gel. The good agreement shown in Fig. 12 confirms that this assignment is reasonable, although here the assignment method is simplified because there are minor Q^4 Si units possibly present in other Si units,[72,73] and Q^2 and Q^3 present in N-A-S-H. By comparing the Si/Al_{entire} and $Si/Al_{Al\ NMR}$ ratios in Fig. 12(b), it can be found that the Si/Al_{entire} ratio value is slightly higher, especially for long-aged N-A-S-H gels. This is due to an overlap of zeolite and gel in the Al spectra as mentioned in Section 3.5.1, causing an overestimation of $I_{Al(IV)\text{-}gel}$. In addition, the Si/Al_{entire} (or $Si/Al_{Al\ NMR}$) ratio above 1.75 is associated with the detectable emergence of C-A-S-H nanostructures (Q^1 and Q^2).

3.5.3 Effects of Ca/Si and Si/Al ratios on Al species. From the above analysis, it is confirmed that Al predominantly exists in tetrahedral coordination within N-A-S-H and C-A-S-H gels. With the increase of calcium concentration, the Al(VI) sites at ~68 and ~58 ppm occur, representing the generation of Q^2 and Q^3, respectively. When the Ca/Si ratio increases to 0.2, calcium initially incorporates into N-A-S-H gel, forming a calcium-containing N(-C)-A-S-H gel phase, of which the nanostructure is still composed of $Q^4(mAl)$ units. As the Ca/Si ratio rises to 0.4–0.5, $Q^2(mAl)$ units occur, accompanied by the possible appearance of $Q^3(mAl)$.

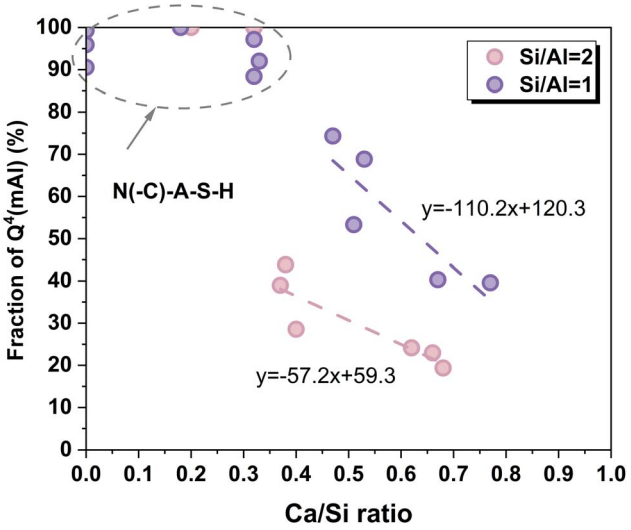

Fig. 13 Effect of the Ca/Si ratio on (a) the fraction of Q^4 with Si/Al = 2 & 1.

Table 3 Chemical shifts δ (ppm) and the fractions (%) of Al in the synthetic gels with Si/Al = 2 obtained from quantitative ^{27}Al NMR spectra analysis[a]

Age (d)	Designed Ca/Si		Al(IV)-a	Al(IV)-b′	Al(IV)-c	Al(IV)-d	Al(VI)-a	Al(VI)-b	Al(VI)-c
1	0	δ			61.7				8.6
		Fraction			99.7				0.3
	0.2	δ			60.9			10.5	
		Fraction			96.2			3.8	
	0.4	δ			60.7	56.6	12.1		7.8
		Fraction			86.5	9.2	1.1		1.1
	0.8	δ	67.2		62.4	58.1	12.1		7.7
		Fraction	8.6		32.8	48.9	4.9		4.8
28	0	δ			61.0				8.5
		Fraction			95.6				4.4
	0.2	δ			60.7				8.3
		Fraction			98.4				1.6
	0.4	δ	67.6		62.4	58.2	12.2		8.7
		Fraction	4.3		24.6	68.6	1.5		1.0
	0.8	δ	68.5	63.2	61.0	57.9	12.2		
		Fraction	4.8	13.7	28.3	34.4	18.9		
90	0	δ			61.3				8.2
		Fraction			89.3				10.6
	0.2	δ			60.7		12.1		7.5
		Fraction			98.0		1.0		0.9
	0.4	δ	66.1		61.4	57.8	12.2		8.2
		Fraction	8.5		21.2	67.9	1.2		1.2
	0.8	δ	67.8		61.1	57.1	12.1		
		Fraction	2.5		27.0	69.0	1.5		

[a] Al(IV)-a: Q^2 Al at chain-bridging sites balanced by $\frac{1}{2}Ca^{2+}$ together with H_3O^+ or by H^+ ions; Al(IV)-b′: AFm phase; Al(IV)-c: bridging Q^2 Al (charge-balanced *via* interlayer Ca^{2+} ions or combinations of interlayer Ca^{2+} and Na^+ ions) and Al(IV) species in N-A-S-H gel; Al(IV)-d: the cross-linked Q^3 Al site; Al(VI)-a: AFm phase; Al(VI)-b: AFm phase, calcium aluminate hydrates, katoite, or siliceous hydrogarnets; Al(VI)-c: paragonite.

Although the peak at 5 ppm was initially ascribed to a "third aluminum hydroxide" (TAH) phase, subsequent DFT calculations and DNP NMR measurements have demonstrated that this assignment seems to be incorrect.[74,75] Some researchers have reported that with the increase of the Ca/Si ratio, bridging Al(VI) species emerged and progressively increased in proportion in C-A-S-H gel, which corresponds to the characteristic peaks at 5 and 9 ppm in the ^{27}Al NMR spectra.[59] The peak of gel bridging octahedral aluminate at 5 ppm is not detected in some samples with a relatively small Ca/Si ratio of 0.84. In this study, the resonance at 5 ppm cannot be found. The intensity of the resonance at ~9 ppm decreases with increasing Ca content, which contradicts the trend reported in a previous study. Therefore, the present results suggest the absence of bridging octahedral Al units in the low-calcium high-aluminum gels.

When the Ca/Si ratio changes from 0 to 0.8, the intensity of octahedral Al species keeps rising (or initially declines slightly but subsequently rises). At Si/Al ratio = 2, Al(VI)-a and Al(VI)-b show a greater increase, which is attributed to a significant increase in the calcium-containing secondary phase. At Si/Al ratio = 1, the decline of the total fraction of Al(VI) sites is more obvious with increasing Ca. It is due to the reduction of the calcium-free solid phase (Al(VI)-c) generated in an aluminum-rich environment. Thus, the variation of octahedral Al species results from two competing effects: the increased formation of Ca-containing secondary phases *versus* the decrease of Ca-free solid phase generated with N-A-S-H.

3.5.4 Phase evolution and nanostructure variation. The Si/Al ratios of C-A-S-H and N(-C)-A-S-H gels are respectively presented in Table 7. For the system with a designed Si/Al ratio of 2, the formation of the C-A-S-H gel chain can be observed at 1 day. When the Si/Al ratio is 1, Q^2 and Q^3 occur at 28 days. This indicates that a high concentration of Al^{3+} in solution kinetically retards the formation of C-A-S-H gel. Si/Al_{NASH} slightly decreases with increasing calcium concentration, but $Si/Al_{NC\text{-}CASH}$ and $Si/Al_{C\text{-}CASH}$ are more strongly affected by calcium. This means that calcium has a greater impact on the nanostructure variation of C-A-S-H gel than on the nanostructure variation of N-A-S-H gel.

As reaction time increases, the N(-C)-A-S-H gel proportion decreases and C-A-S-H gel proportion increases, as confirmed in Tables 5 and 6 The decline of Al(VI)-c species at ~61 ppm also indicates the decrease of $Q^4(m\text{Al})$ with increasing Ca. These findings are consistent with the TEM results, demonstrating a time-dependent increase of the Ca/Si ratio in products and the gradual disappearance of N-A-S-H gel. The effect of the Ca/Si ratio on the fraction of $Q^4(m\text{Al})$ is shown in Fig. 13. For Si/Al = 2, the dashed fitting line exhibits a slope approximately 1.93 times steeper (−110.2 *vs.* −57.2) and an intercept roughly 2.03 times higher (−120.3 *vs.* −59.3) than those for Si/Al = 1. The $Q^4(m\text{Al})$ decline slopes at Si/Al = 2 & 1 suggest a Ca-controlled N(-C)-A-S-H gel depolymerization rate, while the doubled slope at higher Si/Al suggests reduced Al inhibition of Ca-induced depolymerization. The decreased intercept also shows a linear dependence on the Si/Al ratio. The differing initial $Q^4(m\text{Al})$

Table 4 Chemical shifts δ (ppm) and the fractions (%) of Al in synthetic gels with Si/Al = 1 obtained from quantitative ^{27}Al NMR spectra analysis[a]

Reaction time (d)	Ca/Si molar ratio		Al(IV)-a	Al(IV)-b	Al(IV)-c	Al(VI)-a	Al(VI)-b	Al(VI)-c
1	0	δ			62.3			
		Fraction			100.0			
	0.2	δ			61.9		10.0	
		Fraction			96.9		3.1	
	0.5	δ			62.3	12.1		9.0
		Fraction			88.7	3.5		7.8
	0.8	δ			61.7	12.1		8.8
		Fraction			87.8	4.4		7.8
28	0	δ			61.2			8.2
		Fraction			84.1			15.9
	0.2	δ			61.2			8.8
		Fraction			92.6			7.4
	0.5	δ			62.0	12.2		9.2
		Fraction			91.3	2.7		6.3
	0.8	δ	65.7	63.3	60.5	12.2		8.4
		Fraction	13.4	1.1	76.0	4.4		5.1
90	0	δ			62.0			7.4
		Fraction			96.6			2.5
	0.2	δ			60.8			8.5
		Fraction			93.0			7.0
	0.5	δ	66.1	62.3	59.9	12.2		8.9
		Fraction	18.9	16.0	58.4	2.5		4.3
	0.8	δ	67.7	63.3	59.7	12.2		8.4
		Fraction	11.1	10.4	68.9	5.1		4.5

[a] Al(IV)-a: Q^2 Al at chain-bridging sites balanced by $\frac{1}{2}Ca^{2+}$ together with H_3O^+ or by H^+ ions; Al(IV)-b: bridging Q^2 Al(IV) species; Al(IV)-c: bridging Q^2 Al (charge-balanced *via* interlayer Ca^{2+} ions or combinations of interlayer Ca^{2+} and Na^+ ions) and Al(IV) species in N-A-S-H gel; Al(VI)-a: AFm phase; Al(VI)-b: AFm phase, calcium aluminate hydrates, katoite, or siliceous hydrogarnets; Al(VI)-c: paragonite.

fractions reflect Al-dependent initial C-A-S-H content at the onset of phase transformation. The comparatively low R^2 values (0.752 and 0.777) could potentially result from interference by calcium-containing secondary phases or measurement errors. By correlating the ^{29}Si NMR-derived $Q^4(m\mathrm{Al})$ fraction with both the initial Si/Al ratio in solution and the experimentally determined Ca/Si ratio, the following predictive equation (eqn (8)) is established. $Q^4(m\mathrm{Al})$ is from N-A-S-H gel and a small amount of zeolite. Prior to reaching the critical Ca/Si ratio, the $Q^4(m\mathrm{Al})$ fraction remains at ~90–100%. This may be attributed to the possible presence of minor Q^1, Q^2, and Q^3 species at the edges of the N-A-S-H structure. The critical Ca/Si ratios are 0.37 and 0.47 at the initial Si/Al ratios of 2 & 1, respectively. It is important to note that this equation may not be valid for systems with lower Si/Al ratios.

$$I_{Q^4} = \begin{cases} 100 - I_{\mathrm{remnants}}, \ 0 \le r_{\mathrm{Ca/Si}} < R_{\mathrm{Ca/Si}} \\ 59.3 \times \left(1 + 1.03\left(\frac{\mathrm{Si}}{\mathrm{Al}} - 1\right)\right) - 57.2 \times \left(1 + 0.93\left(\frac{\mathrm{Si}}{\mathrm{Al}} - 1\right)\right) \\ \times r_{\mathrm{Ca/Si}}, \ R_{\mathrm{Ca/Si}} \le r_{\mathrm{Ca/Si}} \le 0.8 \end{cases} \quad (8)$$

where I_{Q^4}, I_{remnants}, $r_{\mathrm{Ca/Si}}$, and $R_{\mathrm{Ca/Si}}$ are the fraction of $Q^4(m\mathrm{Al})$ (%), the fraction of remnants (Q^0) (%), the detected molar Ca/Si ratio, and the critical Ca/Si ratio, respectively.

After reaching the minimum critical Ca/Si ratio for gel phase transformation, the overall polymerization degree of the gel is simultaneously influenced by the negative effect of Ca and the promotion of Al. At Si/Al = 2 & 1, the measured critical Ca/Si ratios in gels are 0.37 and 0.47. In alkali-silica gels without Al, the C-S-H-type phases occurred at the measured Ca/Si ≥ 0.23.[72] The critical Ca/Si ratio required for gel transformation from N(-C)-A-S-H to C-A-S-H appears to increase slightly with rising Al concentration in solution.

The disappearance of the $Q^3(m\mathrm{Al})$ fraction is observed with the increase of Al concentration. Similar observations are also found in C-A-S-H at a high Ca/Si ratio and a high Si/Al ratio.[59] The crosslinking degree of C-A-S-H gel (corresponding to $Q^3(m\mathrm{Al})$) declines with increasing reaction time and increasing Al concentration in solution.

The Al in calcium-containing secondary phases (Al(VI)-a, Al(VI)-b, and Al(IV)-b′ sites) exhibits instability, showing either a continuous decrease (Ca/Si = 0.4/0.5) or an initial increase, followed by reduction (Ca/Si = 0.8) over reaction time, as shown in Tables 3 & 4. It is in agreement with the observed decrease and then increase of the Q^3 fraction at ~58 ppm in the Al spectra at Si/Al = 2. This suggests that Ca in solution initially partially incorporates into the gel while simultaneously forming a small amount of solid phases, and then mainly migrates into C-A-S-H gel with time. Calcium also plays a crucial role in the evolution of Ca-free Al-rich secondary phases. In the absence of Ca, these phases increasingly form over time. In contrast, when

Table 5 Chemical shifts δ (ppm) and the fractions (%) of Si in synthetic gels with Si/Al = 2 obtained from quantitative ^{29}Si NMR spectra analysis

Age (d)	Ca/Si ratio		Remnants	Q^1	Q^2(1Al)	Q^2	Q^3(1Al)	Q^3	Q^4(4Al)		Q^4(3Al)		Q^4(2Al)		Q^4(1Al)	Q^4(0Al)
1	0	δ							−78.8	−82.0	−85.0	−87.7	−90.5		−93.8	−96.9
		Fraction							10.5	23.5	23.3	18.4	13.7		8.4	2.2
	0.2	δ							−77.9	−81.3	−84.4	−87.6	−91.3		−95.1	−97.0
		Fraction							10.4	15.9	21.4	23.3	18.1		7.7	3.1
	0.4	δ	−74.3	−78.3	−82.6		−86.3	−93.4	−90.0		−97.3		−101.8		−106.5	−111.7
		Fraction	2.9	6.4	19.7		20.8	10.5	20.0		11.4		4.8		5.3	2.3
	0.8	δ	−75.5	−80.0	−82.9	−85.5	−88.4	−94.0	−91.2		−97.2		−101.0			
		Fraction	1.9	14.7	12.5	19.5	16.7	10.5	11.9		8.3		3.9			
28	0	δ	−75.1						−81.2		−84.1		−89.1		−94.3	−100.7
		Fraction	3.9						25.7		34.1		29.4		10.0	0.8
	0.2	δ							−81.9		−84.5		−91.3		−101.6	−110.5
		Fraction							18.1		25.3		39.3		11.4	5.9
	0.4	δ		−79.6	−82.7	−85.7	−89.1	−94.6	−92.1		−97.5		−101.1		−105.2	
		Fraction		8.1	11.9	20.5	19.4	11.5	12.7		7.9		6.0		1.9	
	0.8	δ		−79.5	−82.8	−85.5	−88.8	−95.6	−92.3		−98.7		−101.6		−104.9	−107.3
		Fraction		9.5	17.6	25.5	16.0	8.5	11.5		5.6		3.2		1.9	0.7
90	0	δ							−81.6		−84.4	−88.2	−92.7		−99.0	
		Fraction							30.1		24.7	19.5	23.4		2.4	
	0.2	δ							−79.5	−82.9	−85.9	−88.1	−90.1	−93.0	−96.8	−101.0
		Fraction							10.0	18.7	22.0	8.4	16.1	13.7	9.5	1.7
	0.4	δ		−79.8	−82.8	−85.8	−89.1	−95.0	−91.9		−97.7		−101.1	−104.5	−107.8	−112.1
		Fraction		9.3	10.5	15.6	13.6	12.0	12.3		10.3		6.9	5.0	3.0	1.5
	0.8	δ		−78.9	−82.7	−85.5	−89.2	−95.1	−92.9		−97.3		−101.3			
		Fraction		9.1	18.6	36.2	15.6	1.1	10.3		5.2		3.9			

Table 6 Chemical shifts (δ (ppm)) and the fractions (%) of Si in synthetic gels with Si/Al = 1 obtained from quantitative ^{29}Si NMR spectra analysis

Age (d)	Ca/Si molar ratio		Remnants	Q^1	Q^2(1Al)	Q^2	Q^4(4Al)		Q^4(3Al)	Q^4(2Al)	Q^4(1Al)	Q^4(0Al)
1	0	δ	−76.6				−80.5		−84.5	−88.7	−92.5	−96.4
		Fraction	4.1				25.2		47.6	16.0	6.4	0.7
	0.2	δ					−78.5	−82.2	−85.7	−89.1	−92.8	−95.8
		Fraction					11.2	27.2	25.3	20.7	10.1	5.4
	0.5	δ	−75.8				−79.7	−83.3	−87.0	−90.5	−93.1	−95.7
		Fraction	6.9				20.2	30.2	23.2	10.0	5.2	3.2
	0.8	δ	−75.8		−82.2		−79.0	−85.4	−87.8	−90.2	−93.0	−96.4
		Fraction	3.4		22.3		13.3	23.1	9.5	15.9	7.3	5.2
28	0	δ	−74.3				−79.2	−83.3	−87.0	−90.4	−94.0	−97.8
		Fraction	0.7				16.1	29.7	25.4	16.5	8.3	3.2
	0.2	δ	−75.9				−79.9	−83.7	−87.6	−91.9	−95.6	
		Fraction	2.8				19.4	32.2	29.2	13.6	2.8	
	0.5	δ	−75.1		−82.9		−80.0	−85.5	−88.1	−91.2	−94.3	−97.9
		Fraction	11.2		20.0		19.0	16.9	14.7	9.8	5.7	2.7
	0.8	δ		−77.8	−81.5	−85.1	−89.2	−93.0	−96.7	−101.0	−103.6	
		Fraction		14.7	18.0	26.1	21.3	10.7	5.8	2.1	0.4	
90	0	δ	−76.5				−82.2		−86.2	−89.6	−93.1	−95.7
		Fraction	9.4				39.2		28.7	15.3	5.2	2.2
	0.2	δ	−76.6				−80.7	−84.6	−88.6	−92.1	−96.4	−99.5
		Fraction	8.8				16.8	43.9	16.0	8.4	2.9	0.5
	0.5	δ	−76.0		−81.7			−85.6	−88.8	−91.9	−95.2	−98.2
		Fraction	7.7		33.3			22.9	15.4	9.2	4.4	1.4
	0.8	δ	−76.0	−80.0	−82.4	−85.5	−89.4	−93.8	−98.0	−102.5		
		Fraction	6.2	11.7	16.3	26.3	20.6	12.3	5.9	0.8		

Ca is relatively abundant, their content gradually decreases with age. This indicates the competing effect of the formation of Ca-containing secondary phases *versus* the reduction of Ca-free Al-rich phases.

3.5.5 Factors controlling MCLs and Si/Al ratios

3.5.5.1 Overall products. The Si/Al_{entire} ratio or $Si/Al_{Al\ NMR}$ ratio of gels decreases with the increase of the Al concentration of the mixed solution. The high Al concentration enables C-S-H to absorb Al^{3+} more strongly.[76] Some researchers found that the Si/Al ratio of C-A-S-H gel was dominated mainly by the Al concentration in solution and independent of the Ca solution concentration.[41] However, the Si/Al ratio of C-A-S-H gel varies quite obviously (2.7–8.7) with increasing Ca content under the conditions of a high aluminum content and a low Ca/Si ratio in this paper. Moreover, the Si/A_{entire} ratio of entire gel is also significantly affected by the Ca concentration in solution in this study. This is probably due to the presence of N-A-S-H gel, in which the amount of Ca is extremely low. The presence of Ca causes a reduction in N-A-S-H gel content. When the initial Al concentration in the solution was relatively low and the Ca concentration was relatively high, which prevented the N-A-S-H formation, the minor amounts of N-A-S-H and N(-C)-A-S-H gels

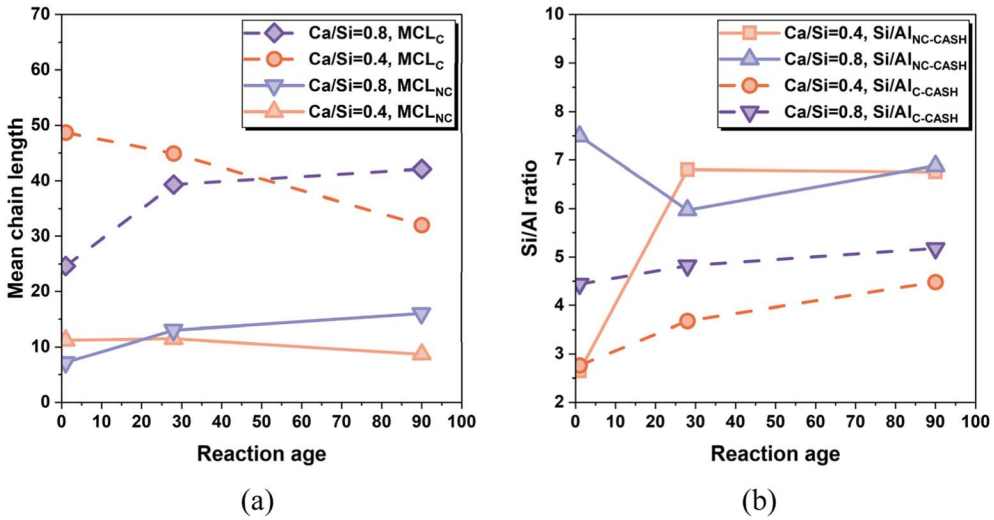

Fig. 14 (a) The crosslinked and non-crosslinked mean chain length (MCL_C and MCL_{NC}), and (b) $Si/Al_{C\text{-}CASH}$ and $Si/Al_{NC\text{-}CASH}$ ratios of synthetic gels with Si/Al = 2 after reaction for 1, 28 and 90 days.

Table 7 Calculated mean chain length (MCL) of C-A-S-H and Si/Al ratios of N-A-S-H and C-A-S-H gels from ^{29}Si & ^{27}Al NMR spectra and TEM-EDS[a]

Si/Al	Age (d)	Ca/Si	MCL_{NC}	$Si/Al_{NC\text{-}CASH}$	MCL_C	$Si/Al_{C\text{-}CASH}$	Si/Al_{NASH}	Si/Al_{entire}	$I_{Al(iv)\text{-}gel}$	$Si/Al_{Al\ NMR}$
2	1	0					1.35	1.35	100%	1.27
		0.2					1.41	1.41	96%	1.57
		0.4	11.2	2.65	48.7	2.76	1.36	1.83	96%	1.78
		0.8	7.2	7.49	24.6	4.44	1.20	2.67	90%	2.85
	28	0					1.46	1.40	96%	1.38
		0.2					1.68	1.68	98%	1.63
		0.4	11.5	6.80	44.9	3.68	1.29	2.41	98%	2.49
		0.8	13.0	5.97	39.3	4.82	1.29	2.96	67%	2.95
	90	0					1.32	1.32	89%	1.41
		0.2					1.46	1.46	98%	1.50
		0.4	8.7	6.75	32.0	4.48	1.46	2.48	98%	2.40
		0.8	16.0	6.88	42.1	5.18	1.20	3.16	99%	2.97
1	1	0					1.36	1.42	100%	1.35
		0.2					1.42	1.42	97%	1.39
		0.5					1.24	1.35	89%	1.43
		0.8	—	2.00			1.39	1.55	88%	1.62
	28	0					1.32	1.33	84%	1.37
		0.2					1.20	1.23	93%	1.34
		0.5	—	2.00			1.29	1.58	91%	1.49
		0.8	9.2	6.55			1.07	2.15	91%	2.04
	90	0					1.30	1.44	97%	0.99
		0.2					1.14	1.29	93%	1.28
		0.5	—	2.00			1.33	1.76	94%	1.80
		0.8	10.7	8.66			1.05	2.27	91%	2.17

[a] Note: the MCL_C and $Si/Al_{C\text{-}CASH}$ were not calculated due to the absence of $Q^3(m\text{Al})$ when the Si/Al ratio is 1.

disappeared with time[23] or were ignored.[63] In an Al-rich and Ca-depleted environment, the presence of N-A-S-H and N(-C)-A-S-H gels cannot be neglected. Thus, the incorporation of Al into overall gels synergistically depends on the concentrations of Ca and Al solutions.

The variation trend of the $Si/Al_{Al\ NMR}$ ratio under different Ca contents is shown in Fig. 12(b). Under low calcium concentrations (Ca/Si $\leq$ 0.2), the $Si/Al_{Al\ NMR}$ ratios of the whole system generally evolve over time to approach the designed Si/Al ratio of the initial solution. This indicates that the Al content in products is mainly controlled by the Al concentration in the solution. In contrast, under relatively high calcium conditions (Ca/Si = 0.4–0.8), the $Si/Al_{Al\ NMR}$ ratios consistently increase with time regardless of the initial Al concentration differences. It was found that with a Ca/(Si + Al) ratio of 0.84, increasing Al content cannot result in an increase in the Al substitution fraction in C-A-S-H gel.[59] Compared with aluminum, calcium seems to be the primary factor determining the mode of the overall developmental trend of the entire Si/Al ratio of gels.

3.5.5.2 N(-C)-A-S-H gel. With the increase of reaction time, the Si/Al_{NASH} ratios of most groups with the Si/Al ratio of 1 change towards the initial Si/Al ratio of the solution; the ratios of the others display a non-monotonic trend, initially rising (or falling) before reversing direction, while remaining bounded around a baseline. The aluminum in N(-C)-A-S-H gel may undergo dynamic exchange with that in the secondary phase, C-A-S-H gel, and the solution. When the concentration of Al in the environment is high, the Si/Al_{NASH} ratio is easily affected by the Al concentration in solution.

3.5.5.3 C-A-S-H gel. The trend of gel MCLs with the target Ca/Si ratios of 0.4 and 0.8 varying with reaction time are is in Fig. 14(a). Calcium concentration leads to different trends in the development of MCLs over time.

At Si/Al = 2, when the Ca/Si ratio is 0.4, as the reaction time increases, the MCLs decrease, accompanied by a reduction in the fraction of $Q^2(1Al)$ and the $Q^3(1Al)$ sites. The proportion reduction of these Al substitution units promotes the shortening of MCLs, although less Q^1 and more $Q^2(m\text{Al})$ can make the chain length longer. When the Ca/Si ratio increases to 0.8, MCLs increase with reaction time. This is mainly due to the significant increase of $Q^2(m\text{Al})$ sites, although $Q^3(m\text{Al})$ slightly decreases and that of $Q^4(m\text{Al})$ remains basically unchanged.

Generally, the Si/Al ratio of gel can characterize some structural features of aluminosilicate chains of C-A-S-H gel. More Al substitution into the aluminosilicate chains can result in a longer MCL. Thus, it can be observed that the $Si/Al_{NC\text{-}CASH}$ ratio (or $Si/Al_{C\text{-}CASH}$ ratio) increases with time and the MCLs decrease with age, except for crosslinked C-A-S-H gel with a Ca/Si ratio of 0.8, as shown in Table 7. This indicates that the influence of Al substitution on MCLs weakens when the Ca/Si ratio increases to 0.8. Moreover, when the reaction time is 1 day, the decrease of $Q^2(1Al)$ and $Q^3(1Al)$ and the increase of Q^1 are the reasons for the decline of MCLs as the Ca/Si ratio increases from 0.4 to 0.8. After 28 days, the increase of $Q^2(m\text{Al})$ sites and the decrease of Q^1 lead to the rise of MCLs with increasing Ca/Si ratio.

In summary, when the Ca content is low (Ca/Si = 0.4), the MCL variation of C-A-S-H gel with age can be mainly determined

by Al substitution in Q^2 and Q^3 Si units. When the Ca content is relatively high (Ca/Si = 0.8), the MCL with age is determined by the fractions of $Q^2(m\text{Al})$ and Q^1 units. In addition, when comparing Al-rich gels with different Ca contents, the fractions of $Q^2(1\text{Al})$ and Q^1 can be decisive factors for non-crosslinked and crosslinked MCLs.

The MCLs of these low calcium C-A-S-H are much longer than those of OPC hydration products with or without supplementary cementitious materials. The incorporation of aluminum also results in a larger layer spacing in C-A-S-H.[77] The MCL_{NC} in cement paste ranged from 4.7 to 3.2 over time with a 30% fly ash replacement ratio[78] and was 3.5–3.6 with 20% fly ash replacement.[79] In Portland cement–metakaolin–limestone blends, the MCL_{NC} increased from 3–3.7 to 4–6 when the hydration time increased from 1 day to 21 days. In 11 Å tobermorite, the MCL_C calculate from the equation given by Myers[24] can be twice the value obtained from the well-known expressions related to C–S–H gel ($MCL = (2 \times (Q^1 + Q^2(0\text{Al}) + 1.5 \times Q^2(0\text{Al}) + Q^3 + Q^3(1\text{Al})))/Q^1$). Thus, the MCL_C of Portland cement-metakaolin-limestone blends varied from 8–14 to 9.6–17.2 when the hydration time changed from 28 to 420 days. Liu *et al.*[80] investigated the hybrid alkaline cement comprising 67.5% fly ash, 27.5% oil well cement, and 5% Na_2SO_4 powder. The MCL_{NC} and MCL_C were approximately 20 and 80, respectively. These values were overestimated because the Q^2 and Q^3 peaks overlapped with the Q^4 peaks. In alkali-activated slag paste, the MCL_{NC} and MCL_C were 4.2–14 and 10–11, respectively.[64] In gels generated from alkali-activation of calcium aluminosilicate precursors with the Ca/Si ratios of 0.95–1.67 and the Al/Si ratios of 0.04–0.16, the MCL_{NC} and MCL_C were 4.3–8.8 and 9.9–26.5, respectively. Compared to the OPC system, the MCL values of the C-A-S-H gels in this study are closer to those in low-Ca hybrid alkaline cement or low/moderate-Ca alkali-activated cement systems due to the relatively high Al content and low Ca content.

4. Conclusions

By adopting a group of advanced characterization techniques, this study reveals the phase evolution, atomic ordering, and nanostructure of synthetic C-A-S-H and N(-C)-A-S-H gels at low Ca/Si and Si/Al ratios. By establishing a quantitative link between the Ca/Si ratio and Q^4 species, this study provides a framework for subsequent research to elucidate the molecular structure of low-Ca high-Al gels and to establish meaningful connections with their macroscopic properties. The main findings can be concluded as follows:

(1) Mechanisms of Al entering C-A-S-H and N(-C)-A-S-H: the incorporation of substituted Al into C-A-S-H gel is significantly inhibited by the Ca concentration in solution while slightly promoted by the Al concentration in solution in the studied high-Al ((Si/Al = 1 & 2) and low-Ca (Ca/Si ≤ 0.8)) environments. When the Ca concentration is low (Ca/Si ≤ 0.2), the total Al content in products is mainly controlled by the Al concentration in solution. At a relatively higher Ca concentration (Ca/Si = 0.4–0.8), the total Al content decreases with reaction time and Ca entering. The substituted Al exists only as Al(IV) in the aluminosilicate chains of crosslinked or non-crosslinked C-A-S-H gel. No obvious evidence of bridging Al(V) and Al(VI) in the framework of gel is found in this study.

(2) Atomic ordering of C-A-S-H and N(-C)-A-S-H: for C-A-S-H, the increase of the Ca/Si ratio improves the molecular crystallinity (ordering) significantly and this ordering trend becomes more evident at a higher Si/Al ratio (less Al). At Ca/Si ≤ 0.5, gels exhibit almost no long-range ordering above 8 Å, confirming their amorphous nature. For N-A-S-H gels, they remain relatively stable over time. The disorder of Si–O and Al–O coordination environments decreases with increasing Al and the atomic arrangement of N-A-S-H gel tends towards the ideal lattice position with time. With increased Al incorporation, there is a reduced Na/Si ratio and potential Na^+ substitution by Al^{3+} in the structure.

(3) MCLs of C-A-S-H molecules: by quantifying the Q^1, $Q^2(m\text{Al})$, $Q^3(m\text{Al})$, and $Q^4(m\text{Al})$ sites, the non-crosslinked and crosslinked MCLs are calculated to be 7.2–16 and 24.6–48.7, respectively. Under low-calcium conditions, MCLs decrease over time, whereas the opposite trend occurs in high-calcium systems. At Ca/Si = 0.4, the Al substitution in Q^2 and Q^3 is crucial for MCLs, while at Ca/Si = 0.8, $Q^2(1\text{Al})$ and Q^1 become the decisive factors. More fundamentally, it is governed by the Ca/Si ratio and the critical Si/Al (=1.75) threshold in the gel. The MCLs of C-A-S-H molecules are much higher than those in OPC and closer to those in low-Ca hybrid alkaline cement or low/moderate-Ca alkali-activated cement systems.

Conflicts of interest

There are no conflicts to declare.

Data availability

The data are available on request.

Supplementary information (SI) is available. See DOI: https://doi.org/10.1039/d5ta09930g.

Acknowledgements

This research was funded by the National Natural Science Foundation of China (52378257 and U2001225), Fundamental Research Funds for the Central Universities (22120250415), Open Funds of Ningbo Institute of Materials Technology and Engineering Chinese Academy of Sciences, and Funds of Geopoly ® New Materials Company. We thank the Shanghai Synchrotron Radiation Facility of BL14B1 (https://cstr.cn/31124.02.SSRF.BL14B1) for assistance with X-ray scattering measurements. Z. Z. also acknowledges the project of the Industry Information-Science & Technology Department of Hangjinqi, Inner Mongolia (2024HGJ12).

References

1 M. A. Gómez-Casero, L. Pérez-Villarejo, P. J. Sánchez-Soto and D. Eliche-Quesada, *Sustain. Chem. Pharm.*, 2022, **29**, 100746.

2 Y. Deng, Z. Zhang, J. Hu, Q. Yu and C. Shi, *Compos. B Eng.*, 2025, **295**, 112211.
3 J. L. Provis, *Cem. Concr. Res.*, 2018, **114**, 40–48.
4 C. Shi, A. F. Jiménez and A. Palomo, *Cem. Concr. Res.*, 2011, **41**, 750–763.
5 A. Fernández-Jiménez and A. Palomo, *Cem. Concr. Res.*, 2005, **35**, 1984–1992.
6 A. Wang, Y. Zheng, Z. Zhang, K. Liu, Y. Li, L. Shi and D. Sun, *Engineering*, 2020, **6**, 695–706.
7 P. Zhang, Y. Zheng, K. Wang and J. Zhang, *Compos. B Eng.*, 2018, **152**, 79–95.
8 J. Mei, C. Yin, Y. Zhao, Y. Niu, A. Xie and S. Li, *ZKG Int.*, 2024, **77**(8), 42–50.
9 J. Ma and F. Dehn, *Struct. Concr.*, 2017, **18**, 801–810.
10 H. Gao, E. Hamed, I. M. A. Al-Damad, A. Hajimohammadi and S. Foster, *Mater. Struct.*, 2025, **58**, 160.
11 T. Yang, X. Gao, J. Zhang, X. Zhuang, H. Wang and Z. Zhang, *Compos. B Eng.*, 2022, **242**, 110024.
12 H. Ye and A. Radlińska, *Cem. Concr. Res.*, 2016, **88**, 126–135.
13 J. Skibsted and M. D. Andersen, *J. Am. Ceram. Soc.*, 2013, **96**, 651–656.
14 Z. Zhang, Z. Zhou, H. Zhu, P. Duan, Y. Fang and Z. Jiang, *Compos. B Eng.*, 2024, **271**, 111157.
15 Z. Zhou, Z. Zhang, Y. Deng, J. Hu, Q. Yu and C. Shi, *J. Chin. Ceram. Soc.*, 2023, **51**, 2138–2152.
16 M. Delhorme, C. Labbez, M. Turesson, E. Lesniewska, C. E. Woodward and B. Jönsson, *Langmuir*, 2016, **32**, 2058–2066.
17 S. Gaboreau, S. Grangeon, F. Claret, D. Ihiawakrim, O. Ersen, V. Montouillout, N. Maubec, C. Roosz, P. Henocq and C. Carteret, *Langmuir*, 2020, **36**, 9449–9464.
18 J. Li, W. Zhang, K. Xu and P. J. M. Monteiro, *Cem. Concr. Res.*, 2020, **137**, 106195.
19 G. K. Sun, J. F. Young and R. J. Kirkpatrick, *Cem. Concr. Res.*, 2006, **36**, 18–29.
20 Q. Fu and J. Huang, *Prog. Mater. Sci.*, 2026, **159**, 101666.
21 M. Jin, Y. Ma, W. Li, J. Huang, Y. Yan, H. Zeng, C. Lu and J. Liu, *Cem. Concr. Res.*, 2023, **172**, 107251.
22 Z. Li, M. Nedeljković, B. Chen and G. Ye, *Cem. Concr. Res.*, 2019, **122**, 30–41.
23 J. Wang, Z. Hu, Y. Chen, J. Huang, Y. Ma, W. Zhu and J. Liu, *Cem. Concr. Res.*, 2022, **157**, 106811.
24 R. Myers, S. Bernal, R. San Nicolas and J. Provis, *Langmuir*, 2013, **29**, 5294–5306.
25 K. M. L. Alventosa and C. E. White, *J. Phys. Chem. C*, 2024, **128**, 2116–2129.
26 C. E. White, L. L. Daemen, M. Hartl and K. Page, *Cem. Concr. Res.*, 2015, **67**, 66–73.
27 K. Gong and C. E. White, *Cem. Concr. Res.*, 2016, **89**, 310–319.
28 I. Garcia-Lodeiro, A. Palomo, A. Fernández-Jiménez and D. E. Macphee, *Cem. Concr. Res.*, 2011, **41**, 923–931.
29 L. Qin, B. Qu, C. Shi and Z. Zhang, *Mater. Rep.*, 2020, **34**, 12057–12063.
30 B. Walkley, R. San Nicolas, M.-A. Sani, G. J. Rees, J. V Hanna, J. S. J. van Deventer and J. L. Provis, *Cem. Concr. Res.*, 2016, **89**, 120–135.
31 P. Martín-Rodríguez, I. García-Lodeiro, L. Fernández-Carrasco, M. T. Blanco-Varela, A. Palomo and A. Fernández-Jiménez, *Compos. B Eng.*, 2025, **296**, 112216.
32 Q. Wan, F. Rao, S. Song, R. E. García, R. M. Estrella, C. L. Patiño and Y. Zhang, *Cem. Concr. Compos.*, 2017, **79**, 45–52.
33 I. García-Lodeiro, A. Fernández-Jiménez, M. T. Blanco, A. Palomo and J. Solgel, *Sci. Technol.*, 2008, **45**, 63–72.
34 Y. Chen, L. M. de Lima, Z. Li, B. Ma, B. Lothenbach, S. Yin, Q. Yu and G. Ye, *Cem. Concr. Res.*, 2024, **180**, 107484.
35 A. P. Hammersley, S. O. Svensson, M. Hanfland, A. N. Fitch and D. Hausermann, *High Press. Res.*, 1996, **14**, 235–248.
36 P. Juhás an, T. Davis, C. L. Farrow and S. J. L. Billinge, *J. Appl. Crystallogr.*, 2013, **46**, 560–566.
37 F. S. Hashem, O. Fadel, F. A. Selim and H. S. Hassan, *Sustain. Chem. Pharm.*, 2025, **43**, 101890.
38 Q. Wang, X. Li, S. Ma, H. Yang, W. Shi, Q. Chang, Y. Wang and H. Jin, *J. Non-Cryst. Solids*, 2025, **650**, 123373.
39 Z. Sun and A. Vollpracht, *Cem. Concr. Res.*, 2018, **103**, 110–122.
40 C. Liu, Y. Tao, S. Nie, Y. Chen, Z. Li, C. S. Poon and G. Ye, *Compos. B Eng.*, 2025, **297**, 112337.
41 E. L'Hôpital, B. Lothenbach, G. Le Saout, D. Kulik and K. Scrivener, *Cem. Concr. Res.*, 2015, **75**, 91–103.
42 R. Si, S. Guo and Q. Da, *J. Am. Ceram. Soc.*, 2019, **102**, 1479–1494.
43 X. Gao, Q. L. Yu and H. J. H. Brouwers, *Ceram. Int.*, 2017, **43**, 12408–12419.
44 T. Egami and S. J. L. Billinge, *Underneath the Bragg Peaks: Structural Analysis of Complex Materials, [S.l.]*, Pergamon, 2nd edn, 2012.
45 L. B. Skinner, S. R. Chae, C. J. Benmore, H. R. Wenk and P. J. M. Monteiro, *Phys. Rev. Lett.*, 2010, **104**(19), 195502.
46 S. Soyer-Uzun, S. R. Chae, C. J. Benmore, H.-R. Wenk and P. J. M. Monteiro, *J. Am. Ceram. Soc.*, 2012, **95**, 793–798.
47 C. E. White, J. L. Provis, B. Bloomer, N. J. Henson and K. Page, *Phys. Chem. Chem. Phys.*, 2013, **15**, 8573–8582.
48 K. Gong and C. E. White, *Cem. Concr. Res.*, 2022, **151**, 106642.
49 A. E. Morandeau and C. E. White, *Chem. Mater.*, 2015, **27**, 6625–6634.
50 K. Garbev, B. Gasharova, A. Ullrich, G. Beuchle and P. Stemmermann, *Cem. Concr. Res.*, 2025, **198**, 108000.
51 S. A. Bernal, J. L. Provis, V. Rose and R. Mejía de Gutierrez, *Cem. Concr. Compos.*, 2011, **33**, 46–54.
52 P. Yu, R. J. Kirkpatrick, B. Poe, P. F. McMillan and X. Cong, *J. Am. Ceram. Soc.*, 1999, **82**, 742–748.
53 Y. Wang, Y. Cao, Z. Zhang, P. Zhang, Y. Ma, A. Wang and H. Wang, *Cem. Concr. Res.*, 2023, **165**, 107068.
54 I. García Lodeiro, A. Fernández-Jimenez, A. Palomo and D. E. Macphee, *Cem. Concr. Res.*, 2010, **40**, 27–32.
55 Z. Zhang, H. Wang and J. L. Provis, *J. Sustain. Cem.-Based Mater.*, 2012, **1**, 154–166.
56 M. Sitarz, M. Handke, W. Mozgawa, E. Galuskin and I. Galuskina, *J. Mol. Struct.*, 2000, **555**, 357–362.
57 B. Walkley, R. San Nicolas, M.-A. Sani, J. D. Gehman, J. S. J. van Deventer and J. L. Provis, *Powder Technol.*, 2016, **297**, 17–33.

58 F. Puertas, S. Martínez-Ramírez, S. Alonso and T. Vázquez, *Cem. Concr. Res.*, 2000, **30**, 1625–1632.
59 X. Zhu, M. Vandamme, L. Brochard, Z. Zhang, Q. Ren, C. Li, B. He, H. Zhang, Y. Zhang, Q. Chen and Z. Jiang, *Cem. Concr. Res.*, 2023, **167**, 107131.
60 L. Kobera, J. Brus, P. Klein, J. Dedecek and M. Urbanova, *Solid State Nucl. Magn. Reson.*, 2014, **57–58**, 29–38.
61 B. Walkley, G. J. Rees, R. San Nicolas, J. S. J. van Deventer, J. V Hanna and J. L. Provis, *J. Phys. Chem. C*, 2018, **122**, 5673–5685.
62 J. Brus, L. Kobera, M. Urbanová, D. Koloušek and J. Kotek, *J. Phys. Chem. C*, 2012, **116**, 14627–14637.
63 S.-Y. Yang, Y. Yan, B. Lothenbach and J. Skibsted, *J. Phys. Chem. C*, 2021, **125**, 27975–27995.
64 R. J. Myers, S. A. Bernal, J. D. Gehman and J. L. Provis, *J. Am. Ceram. Soc.*, 2015, **98**, 996–1004.
65 M. J. A. Qomi, F. Ulm and R. J.-M. P. Pellenq, *J. Am. Ceram. Soc.*, 2012, **95**, 1128–1137.
66 B. Walkley, R. San Nicolas, M. A. Sani, J. D. Gehman, J. S. van Deventer and J. L. Provis, *Dalton Trans.*, 2016, **45**, 5521–5535.
67 I. García-Lodeiro, A. Fernández-Jiménez, A. Palomo and D. E. Macphee, *J. Am. Ceram. Soc.*, 2010, **93**, 1934–1940.
68 A. Buchwald, H. Hilbig and C. Kaps, *J. Mater. Sci.*, 2007, **42**, 3024–3032.
69 L. Xue, Z. Zhang and H. Wang, *Cem. Concr. Compos.*, 2021, **123**, 104200.
70 S. A. Bernal, J. L. Provis, B. Walkley, R. San Nicolas, J. D. Gehman, D. G. Brice, A. R. Kilcullen, P. Duxson and J. S. J. van Deventer, *Cem. Concr. Res.*, 2013, **53**, 127–144.
71 J. L. Provis, P. Duxson, G. C. Lukey and J. S. J. van Deventer, *Chem. Mater.*, 2005, **17**, 2976–2986.
72 M. E. Krüger, A. Heisig, H. Hilbig, H. Eickhoff, D. Heinz and A. Machner, *Cem. Concr. Res.*, 2023, **166**, 107088.
73 L. Irbe, *Doctoral Dissertation*, Technische Universität München, 2019.
74 M. D. Andersen, H. J. Jakobsen and J. Skibsted, *Inorg. Chem.*, 2003, **42**, 2280–2287.
75 A. Kunhi Mohamed, P. Moutzouri, P. Berruyer, B. J. Walder, J. Siramanont, M. Harris, M. Negroni, S. C. Galmarini, S. C. Parker, K. L. Scrivener, L. Emsley and P. Bowen, *J. Am. Chem. Soc.*, 2020, **142**, 11060–11071.
76 B. Lothenbach and A. Nonat, *Cem. Concr. Res.*, 2015, **78**, 57–70.
77 W. Cai, Z. Xu, Z. Zhang, J. Hu, H. Huang, Y. Ma, Z. Zhang, H. Wang, S. Yin, J. Wei, C. Shi and Q. Yu, *Compos. B Eng.*, 2022, **238**, 109919.
78 J. Li, X. Liu, Q. Yang, D. Hou, X. Hu, Q. Ye, D. Wang and Q. Ding, *Constr. Build. Mater.*, 2020, **262**, 120823.
79 C. Luan, Z. Wu, Z. Han, X. Gao, Z. Zhou, P. Du, F. Wu, S. Du and Y. Huang, *J. Clean. Prod.*, 2023, **415**, 137735.
80 T. Liu, G. Zhao, B. Qu and C. Gong, *Constr. Build. Mater.*, 2024, **445**, 137874.